Geological Magazine

www.cambridge.org/geo

Late Palaeozoic tectonic evolution of the eastern Palaeo-Asian Ocean: new evidence from the early Permian arc magmatic suites in the Kulun region

Yan Jing[1,2], Wen-chun Ge[1,2], Hao Yang[1,2], Yu Dong[1,2], Zheng Ji[1,2], Jun-hui Bi[3], Hong-ying Zhou[3] and Dehe Xing[4]

[1]College of Earth Sciences, Jilin University, Changchun 130061, China; [2]Key Laboratory of Mineral Resources Evaluation in Northeast Asia, Ministry of Land and Resources of China, Changchun 130026, China; [3]Tianjin Centre of the China Geological Survey, Tianjin 300170, China and [4]Shenyang Centre of the China Geological Survey, Shenyang 110034, China

Original Article

Cite this article: Jing Y, Ge WC, Yang H, Dong Y, Ji Z, Bi JH, Zhou HY, and Xing D (2022) Late Palaeozoic tectonic evolution of the eastern Palaeo-Asian Ocean: new evidence from the early Permian arc magmatic suites in the Kulun region. *Geological Magazine* **159**: 1513–1528. https://doi.org/10.1017/S0016756822000358

Received: 2 June 2021
Revised: 5 April 2022
Accepted: 12 April 2022
First published online: 20 July 2022

Keywords:
Central Asian Orogenic Belt; Kulun region; early Permian; felsic magmatic suites; southward subduction; Palaeo-Asian Ocean

Author for correspondence:
Wen-chun Ge,
Email: gewenchun@jlu.edu.cn

Abstract

Late Palaeozoic igneous rock associations in response to subduction, accretion, and final closure of the eastern Palaeo-Asian Ocean play a significant role in understanding the geodynamic evolution of the southeastern Central Asian Orogenic Belt. Previous studies have identified a Permian arc magmatic belt associated with the southward-dipping subduction of the eastern Palaeo-Asian Ocean along the Solonker–Changchun suture zone. The genetic mechanism and associated geodynamic settings are of great importance in deciphering the evolution of the eastern Palaeo-Asian Ocean. This paper presents zircon U–Pb–Hf isotope and whole-rock geochemical analyses for a suite of magmatic rocks including the early Permian diorite porphyrites (*ca*. 281.0 Ma), andesites (*ca*. 276 Ma) and rhyolites (*ca*. 275 Ma) in the Kulun region. The diorite porphyrites and andesites have high SiO_2 and total alkali contents, and low MgO contents and Mg no. values, with enrichments in large ion lithophile elements and depletions in high-field-strength elements. These geochemical characteristics, together with low-Sr and high-Yb contents, a weak concave-upward shape of middle rare earth elements and negative Eu anomalies, suggest that these intermediate igneous rocks were generated by partial melting of amphibolitic lower crust at a crustal depth of 30–40 km. The rhyolites have heterogeneous isotopic compositions, with $\epsilon_{Hf}(t)$ values and T_{DM2} ages of –20.8 to +0.5 and 3578~1494 Ma, implying that they were likely derived from partial melting of a mixed source dominated by recycled ancient crust with minor juvenile crustal materials. The rhyolites show potassic affinity with relatively high K_2O and very low Na_2O, which was attributed to liquid immiscibility of felsic magma and subsequent limited fractional crystallization of plagioclase. The regional igneous associations, metamorphic events, and coeval sedimentary rocks along the Solonker–Changchun suture zone indicate that the early Permian igneous rocks were formed in an active continental arc environment in response to southward subduction of the eastern Palaeo-Asian Ocean.

1. Introduction

Tectonic movement and crust–mantle interactions are most intense in subduction zones on the Earth. Subduction-related igneous rocks, as the most striking characteristics of orogenic systems, hold a key to monitoring important geodynamic processes within orogenic belts (Xiao *et al.* 2003; Annen *et al.* 2006; Li, 2006; Wu *et al.* 2011; Wilde, 2015). The Central Asian Orogenic Belt (CAOB) is regarded as one of the largest and most complicated Phanerozoic accretionary orogenic belts on the Earth, which extends thousands of kilometres from the Urals in the west, through Kazakhstan, northern China and Mongolia to the Okhotsk Sea in the east (Sengör *et al.* 1993; Xiao *et al.* 2003; Li, 2006; Zhou, J. B. *et al.* 2010, 2018; Wilde, 2015; Eizenhöfer & Zhao, 2018; Chai *et al.* 2020; Li *et al.* 2021; Liu *et al.* 2021; Hui *et al.* 2021). Previous studies have revealed that the geodynamic evolution of the CAOB is controlled by subduction, accretion, and closure processes of the Palaeo-Asian Ocean, involving a series of ophiolites, accretionary wedges, accretionary complexes, magmatic arcs, oceanic plateaus and micro-continental blocks (Fig. 1a; Sengör *et al.* 1993; Jahn *et al.* 2000; Badarch *et al.* 2002; Windley *et al.* 2007; Zhou *et al.* 2010; Wu *et al.* 2011; Xiao *et al.* 2015; Wilde, 2015; Eizenhöfer & Zhao, 2018; Chai *et al.* 2020; Hui *et al.* 2021; Yang *et al.* 2022). Along with the consumption and final closure of the Palaeo-Asian Ocean, the CAOB was ultimately assembled along the northern margin of the Tarim and North China cratons (Xiao *et al.* 2015; Eizenhöfer & Zhao, 2018; Hui *et al.* 2021). It is widely accepted that the final closure of the eastern Palaeo-Asian Ocean is recorded by the Solonker–Changchun suture zone, separating the

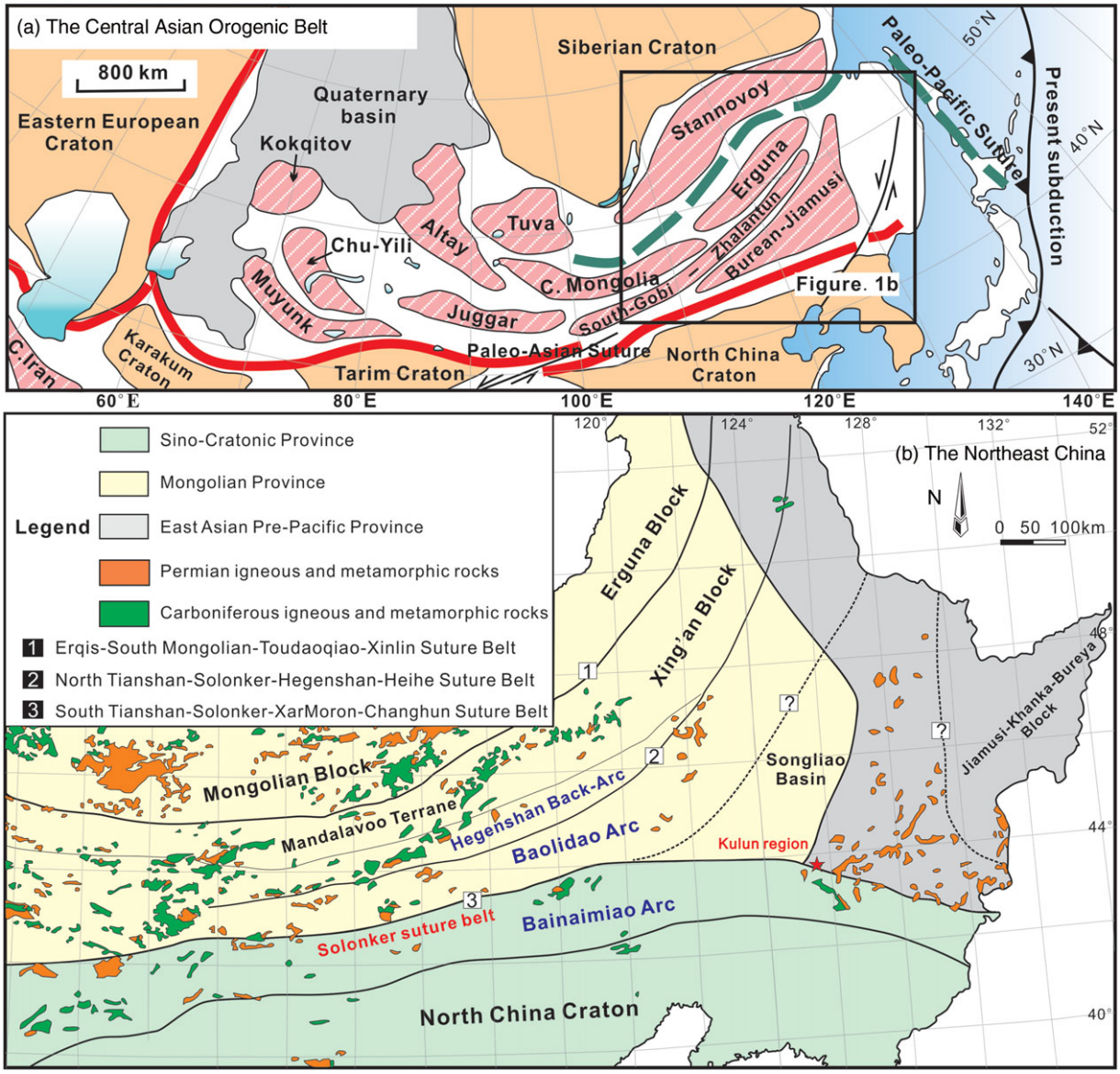

Fig. 1. (Colour online) (a) Tectonic sketch map of the southeastern Central Asian Orogenic Belt (modified after Li, 2006). (b) Geological sketch map of NE China (modified after Eizenhöfer & Zhao, 2018).

North China Craton (NCC) to the south from the amalgamated blocks of northeast (NE) China to the north (Xiao *et al.* 2003; Li, 2006; Zhou, J. B. *et al.* 2010, 2018; Wilde, 2015; Eizenhöfer & Zhao, 2018; Chai *et al.* 2020; Liu *et al.* 2021). Since typical collision-related features do not develop, the detailed geodynamic processes involved in the final closure are controversial and ocean closure time is uncertain, with it spanning from Devonian to Middle Triassic times. The first model argues that the final closure of the eastern Palaeo-Asian Ocean occurred during early to middle Devonian time by bi-directional subduction, based on the Baolidao and Bainaimiao arc-accretion complexes in southern Mongolia and central Inner Mongolia, respectively (Xu *et al.* 2013). The Carboniferous and Permian–Triassic magmatic rocks along the Solonker–Changchun suture zone are interpreted to have formed in an extensional tectonic environment in response to post-orogenic or mantle plume-related geologic events (Xu *et al.* 2013). The second model proposes that the final ocean closure took place prior to early Permian time (Zhao *et al.* 2020), which resulted from palaeomagnetic data from the early Permian volcanic strata in the Bayandun region of northeastern Mongolia. The third model advocates that the final closure of the eastern Palaeo-Asian Ocean occurred in latest Permian or earliest Middle Triassic time along the Solonker–Changchun suture zone, following a prolonged history of subduction and accretion (Xiao *et al.* 2003; Li, 2006; Wu *et al.* 2007, 2011; Cao *et al.* 2011, 2013; Yu *et al.* 2014; Eizenhöfer *et al.* 2014; Yuan *et al.* 2016; Guo *et al.* 2016; Liu, J. *et al.* 2016, 2020; Huang *et al.* 2018; Song *et al.* 2018; Eizenhöfer & Zhao, 2018; Imayama *et al.* 2019; Jing *et al.* 2020*a*,*b*; Liu *et al.* 2021). Global plate reconstructions for the Triassic to present conducted by Müller *et al.* (2019) also prefer a late Permian–Triassic closure of the Palaeo-Asian Ocean. These continued accretion and collision processes resulted in the development of late Carboniferous – Early Triassic E–W-trending calc-alkaline magmatism and minor high-alkali arc-related volcanic rocks on both sides of the Solonker–Changchun suture zone (Fig. 1b; online Supplementary Material Table S1; Wu *et al.* 2011; Li *et al.* 2014,

https://doi.org/10.1017/S0016756822000358 Published online by Cambridge University Press

2016, 2021; Imayama *et al.* 2019; Liu, J. *et al.* 2020; Jing *et al.* 2020*a*, *b*; Hui *et al.* 2021). The widespread latest late Permian to Middle Triassic adakitic magmatism in the southeastern CAOB marked the final suturing of the Palaeo-Asian Ocean (Li *et al.* 2016), with resultant thickening of the lower crust up to ~59 km (Hui *et al.* 2021). In addition, Wang *et al.* (2021) further proposed another early–middle Permian ridge subduction model based on the formation of multi-type 'abnormal' igneous rocks (282–268 Ma) along the western margin of the Khanka Block. The high heat condition is recorded by the decomposition reactions of magnesite constraints of Mg isotopes and high zircon saturation temperatures of felsic rocks (855–935 °C).

The Kulun region of eastern Inner Mongolia is located in the junction between the southeastern margin of the CAOB and the northern margin of the NCC. During final-stage evolution of the eastern Palaeo-Asian Ocean, subduction, accretion, final closure or/and collision triggered a suites of tectono-magmatic events and relevant crust–mantle interactions, which were well documented in magmatic rocks. Thus, understanding the petrogenesis of late Palaeozoic igneous rocks occurring in the northern margin of the NCC is pivotal to determining the amalgamation processes of the CAOB and the subduction to final closure history of the eastern Palaeo-Asian Ocean. Previous studies have shown that felsic rocks are widely distributed along the Solonker–Changchun suture zone (Zhang, X. H. *et al.* 2010; Liu, J. *et al.* 2016, 2020; Jing *et al.* 2020*a*,*b*). Understanding the emplacement history of these granitic rocks and their volcanic equivalents is essential for establishing the magmatic and geodynamic evolution of the southeastern CAOB (Cao *et al.* 2011, 2013; Yu *et al.* 2014; Li *et al.* 2014, 2016; Liu, J. *et al.* 2016, 2020; Song *et al.* 2018; Jing *et al.* 2020*a*,*b*; Li *et al.* 2021; Hui *et al.* 2021). This is especially true for the Kulun region, which is distinguished by voluminous intermediate-acidic igneous rocks. Field observations of these magmatic rocks have identified a suite of andesites, rhyolites and diorite porphyrites. From previous studies, the late Palaeozoic magmatic rocks distributed along the Solonker–Changchun suture zone are mostly calc-alkaline; however, potassic rhyolites with distinctive geochemical and isotopic compositions have now been identified in the Kulun region (Fig. 2). Petrogenetic models proposed for these rhyolites with potassic affinity, although somewhat unclear and controversial, mainly involve the partial melting of crustal materials in active magmatic arc and continental intraplate environments. Identifying and characterizing the late Palaeozoic magmatic rocks in the Kulun region might provide insights into the geodynamic evolution of the eastern Palaeo-Asian Ocean.

In this contribution, zircon U–Pb analyses and whole-rock elemental and *in situ* zircon Hf isotopic compositions are presented for the late Palaeozoic igneous rocks of the Kulun region of the Solonker–Changchun suture zone. The aim of the study is to establish the emplacement ages, petrogenesis and source characteristics of these igneous rocks, thus elucidating subduction, accretion and reworking processes of the continental crust during late Palaeozoic time.

2. Geological background and sample descriptions

The formation of the Palaeo-Asian Ocean commenced in early Neoproterozoic time, following the break-up of the Rodinia supercontinent (Khain *et al.* 2003; Cawood *et al.* 2013). The consumption, accretion and final closure of the Palaeo-Asian Ocean led to the formation of the CAOB, including the amalgamations of the North China and Tarim cratons to the south, the East European and Siberian cratons to the north, and micro-continental blocks, island arcs and accretionary wedge (Sengör *et al.* 1993; Jahn *et al.* 2000; Li, 2006; Zhou, J. B. *et al.* 2010, 2018; Wilde, 2015; Eizenhöfer & Zhao, 2018; Chai *et al.* 2020; Li *et al.* 2021; Liu *et al.* 2021; Hui *et al.* 2021; Wu *et al.* 2021). The NE China region in the southeastern segment of the CAOB (Fig. 1a, b; Xiao *et al.* 2003; Li, 2006) had experienced complicated assembling processes of several microcontinents, involving the Jiamusi Block in the east, the Xing'an and Songnen–Zhangguangcai blocks in central parts, and the Erguna Block in the northwest (Xiao *et al.* 2003, 2009; Li, 2006; Zhou, J. B. *et al.* 2010, 2018; Wilde, 2015). The Erguna Block is proposed to have collided with the Xing'an Block along the Tayuan–Xiguitu suture zone during the early Palaeozoic period, forming the united Erguna–Xing'an block (Ge *et al.* 2005). This composite block then collided with the Songnen–Zhangguangcai Range Block along the Hegenshan–Heihe suture zone, although the timing of this collision event remains controversial (Badarch *et al.* 2002; Li, 2006; Zhou, J. B. *et al.* 2010, 2018). Previous researches focusing on the Hegenshan–Heihe suture indicated that the final collision occurred in middle Palaeozoic time, followed by lithospheric extension of the northwestern Songnen–Zhangguangcai Block in the late Palaeozoic period (Bao *et al.* 1994; Robinson *et al.* 1999; Nozaka & Liu, 2002). Recent studies, however, have proposed that the final collision did not occur prior to early Permian time, but instead in latest Permian or earliest Triassic time (Miao *et al.* 2008; Yu *et al.* 2017). Furthermore, the amalgamation of the Songnen–Zhangguangcai and Jiamusi blocks is evidenced by the Heilongjiang Complex, a N–S belt extending from Luobei through Yilan to Mudanjiang in Heilongjiang Province (Dong *et al.* 2018). The final amalgamation of these two eastern units mainly occurred during earliest Cretaceous time by the divergent double subduction of the Mudanjiang oceanic plate (Dong *et al.* 2018). The Nadanhada Terrane is generally regarded as an accretionary complex of the Mino–Sikhote Alin terrane related to low-latitude subduction of the Palaeo-Pacific Plate (Wilde, 2015; Zhou, J. B. *et al.* 2018; Lan *et al.* 2022).

The late Palaeozoic igneous rock samples analysed in this study were previously assigned to the Ordovician Kulun Formation (Fig. 3), and comprise mainly andesites, rhyolites, and diorite porphyrites. A nearly 8 m wide diorite porphyrite occurring in the Kulun region is shown in Figure 4a, b. The diorite porphyrite samples have a porphyritic texture and massive structure, and contain phenocrysts (~15 vol. %) of plagioclase, quartz, and alkali feldspar, with accessory minerals of titanite, apatite, and zircon. The groundmass has a cryptocrystalline structure and mineral components similar to the phenocrysts (Fig. 4c, d). The andesite is grey-white and displays a porphyritic texture and massive structure, with phenocrysts (~8 vol. %) of plagioclase and minor amphibole (Fig. 4e, f). The rhyolite occurs in layers in the field outcrops (Fig. 4g) and has a porphyritic texture (Fig. 4h), consisting of phenocrysts (~10 vol. %) of alkali feldspar and quartz, with a felsic groundmass (Fig. 4i, j). The groundmass is dominated by plagioclase and cryptocrystalline materials (Fig. 4i, j). Furthermore, there are also extensive pyroclastic rocks in the field outcrops of the Kulun region (Fig. 4k, l).

3. analytical methods

The measurement of U–Th–Pb isotopes for the volcanic rock samples (17KL14, 17KL19 and 17KL24) and diorite porphyrite sample (16KL012) were carried out by laser ablation inductively coupled

https://doi.org/10.1017/S0016756822000358 Published online by Cambridge University Press

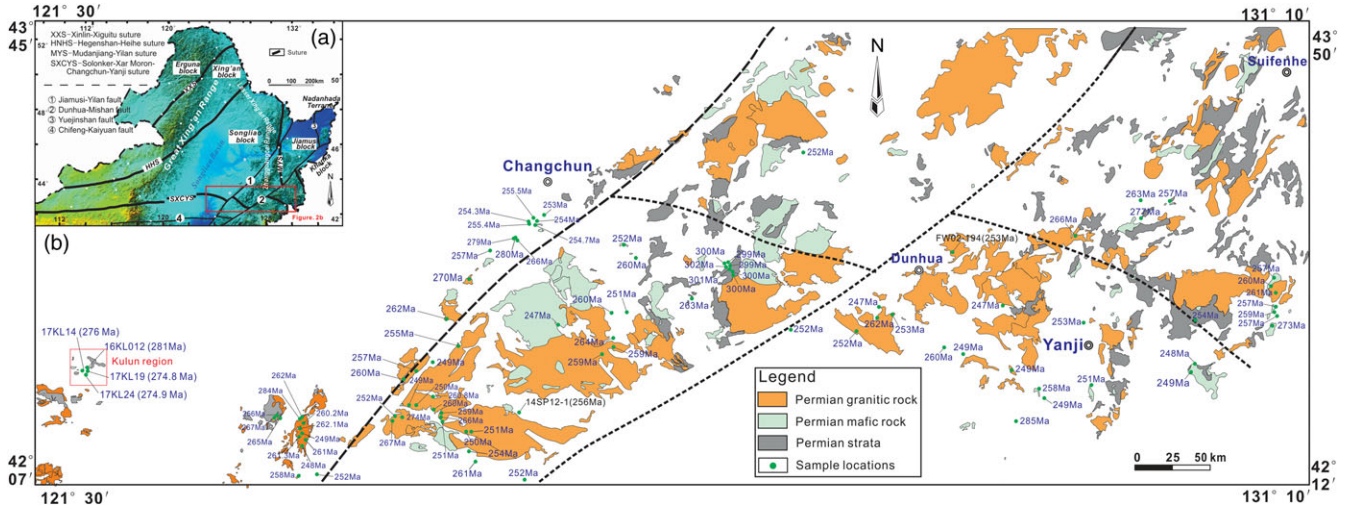

Fig. 2. (Colour online) Geological sketch map and distribution of the late Palaeozoic magmatic rocks along the Solonker–Changchun suture zone. Numbers show all these reported age locations mentioned in online Supplementary Material Table S1.

plasma mass spectrometry (LA-ICP-MS). Geochemical analyses for the diorite porphyrite samples and volcanic rock samples were conducted by X-ray fluorescence (XRF). Hf isotope analyses for all these samples were performed by multi-collector (MC)-ICP-MS (Fig. 5). More detailed descriptions of the analytical procedures are presented in online Supplementary Material S1.

4. Analytical results

4.a. Zircon U–Pb dating and in situ *zircon Hf isotope analyses*

Four representative diorite porphyrite, andesite, and rhyolite samples were selected for zircon U–Pb and Lu–Hf analyses, with the data presented in online Supplementary Material Tables S2 and S3. All these selected zircons have relatively high Th/U ratios (online Supplementary Material Table S2), implying a magmatic origin (Koschek, 1993). The cathodoluminescence (CL) images of zircons from the late Palaeozoic magmatic rocks and associated concordia plots are presented in Figures 6 and 7. It is worth noting that some discordant U–Pb zircon ages show a higher $^{207}Pb/^{235}U$ ratio, which was probably affected by radioactive Pb-loss in zircon.

Sample 16KL012 is diorite porphyrite collected from the northern quarry in the Kulun region. The $^{206}Pb–^{238}U$ ages of 20 analytical points range from 1946 Ma to 279 Ma (online Supplementary Material Table S2), and yield a weighted mean $^{206}Pb–^{238}U$ age of 281.0 ± 1.7 Ma ($n = 10$; MSWD = 1.3) (Fig. 7a), which is considered the crystallization age of the diorite porphyrite. The older zircons varying from 1946 to 296 Ma are considered to be captured zircons. The 403–296 Ma zircons probably come from earlier Carboniferous to Devonian magmatic rocks, whereas the 1946–1876 Ma zircons are more likely from the ancient NCC. The $^{176}Hf/^{177}Hf$ ratios of ten zircon grains from the early Permian (~281 Ma) diorite porphyrite vary from 0.282529 to 0.282880. Their $\epsilon_{Hf}(t)$ values and T_{DM2} ages range from −2.6 to +9.7 and from 1466 to 684 Ma, respectively (Fig. 8a, b; online Supplementary Material Table S3).

Sample 17KL14 is andesite collected from the northern quarry in the Kulun region. LA-ICP-MS zircon U–Pb analysis results show the $^{206}Pb–^{238}U$ ages of 23 analytical points vary from 2149 to 275 Ma (online Supplementary Material Table S2). Only three zircon results yield $^{206}Pb–^{238}U$ ages of 276 ± 5 Ma, 275 ± 5 Ma and 275 ± 5 Ma (Fig. 7b), which are interpreted as the crystallization age of the andesite (*ca.* 276 Ma). The other zircons ranging from 376 to 301 Ma and 2149 to 1814 Ma are considered to be captured zircons, which probably come from the earlier Carboniferous magmatic rocks and southern ancient NCC.

Sample 17KL19 is rhyolite collected from the western quarry in the Kulun region. The $^{206}Pb–^{238}U$ ages for 23 analytical points are in the range of 1910 to 271 Ma (online Supplementary Material Table S2), and yield a weighted mean $^{206}Pb–^{238}U$ age of 274.8 ± 0.9 Ma ($n = 22$; MSWD = 0.54; Fig. 7c). This weighted mean age represents the crystallization time of the rhyolite. The older *c.* 1910 Ma zircon is probably from the ancient NCC. The $^{176}Hf/^{177}Hf$ ratios of 18 zircon grains from the early Permian (~275 Ma) rhyolite vary from 0.282727 to 0.282786. Their $\epsilon_{Hf}(t)$ values and T_{DM2} ages vary from −1.6 to +0.5 and from 1683 to 1494 Ma, respectively (Fig. 8a, b; online Supplementary Material Table S3).

Sample 17KL24 is rhyolite collected from the western quarry in the Kulun region. Twenty-five spots conducted on 25 zircon grains produced $^{206}Pb–^{238}U$ ages varying from 2465 Ma to 271 Ma (online Supplementary Material Table S2), and yielded a weighted mean $^{206}Pb–^{238}U$ age of 274.9 ± 0.8 Ma ($n = 24$, MSWD = 0.35) (Fig. 7d), which represents the time of volcanic eruption. The other zircon with a $^{206}Pb–^{238}U$ age of 2465 ± 27 Ma is regarded as a captured zircon from the southern NCC. The $^{176}Hf/^{177}Hf$ ratios for 18 zircon grains from the early Permian (~275 Ma) rhyolite range from 0.282024 to 0.282361. Their $\epsilon_{Hf}(t)$ values and T_{DM2} ages vary from −20.8 to −9.0 and from 3578 to 2524 Ma, respectively (Fig. 8a, b; online Supplementary Material Table S3).

4.b. Geochemistry

4.b.1. Andesites of the Kulun Formation

The analysed andesites of the Kulun Formation have SiO_2 = 58.80–62.36 wt %, MgO = 1.44–1.51 wt %, Al_2O_3 = 14.03–17.10 wt % and TiO_2 = 0.64–0.97 wt % contents, with aluminium saturation index (A/CNK = molecular $Al_2O_3/(CaO + Na_2O + K_2O)$) values of 0.45 to 1.15 (Fig. 5c; online Supplementary Material Table S4). The total rare earth element (ΣREE) contents of these andesites are 120.0–187.6 ppm, with $(La/Yb)_N$ and δEu values ranging from 5.68 to

https://doi.org/10.1017/S0016756822000358 Published online by Cambridge University Press

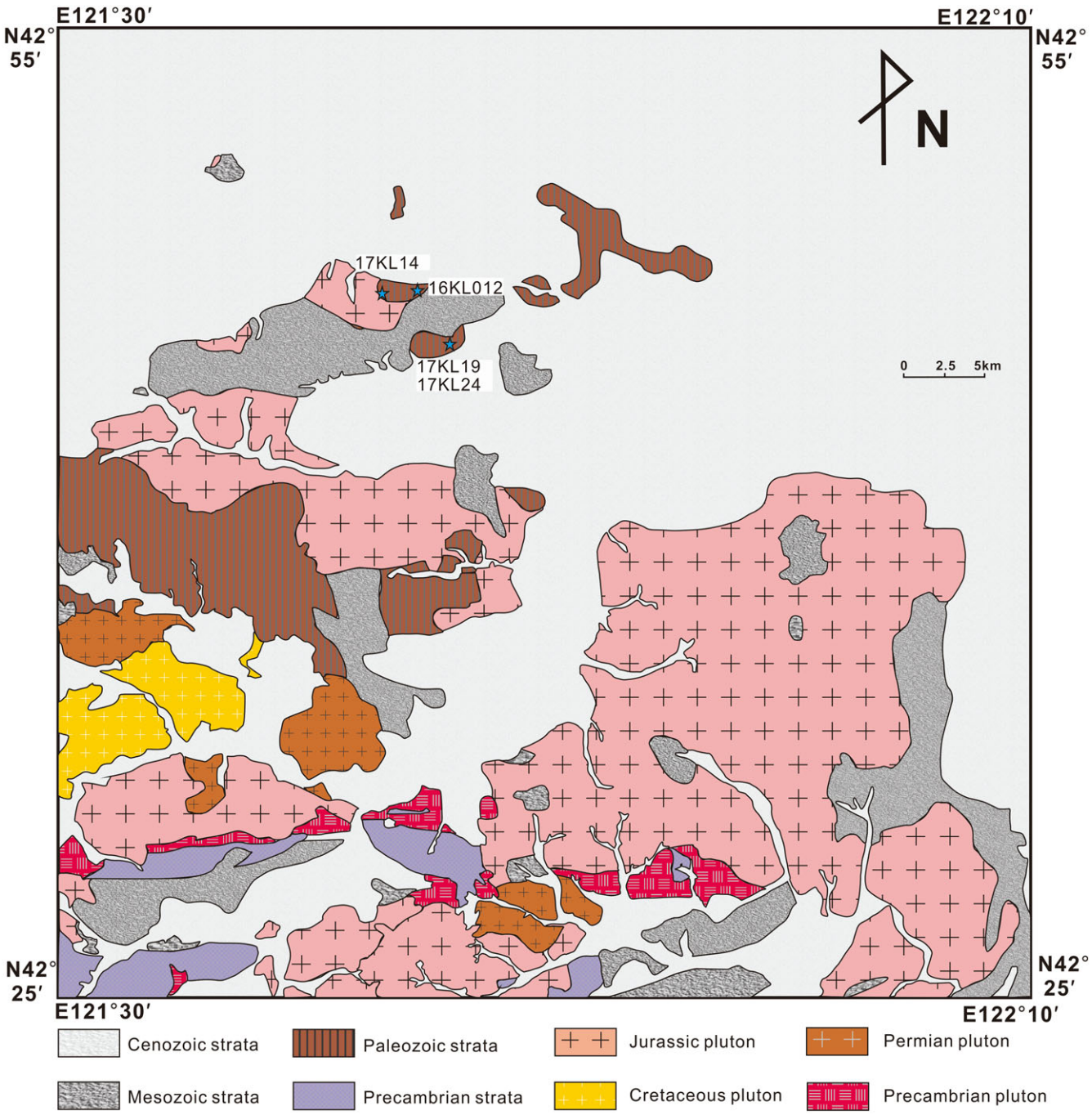

Fig. 3. (Colour online) Geological sketch map of the Kulun region, with the sample locations shown.

9.53, and 0.68 to 0.76, respectively (Fig. 9b; online Supplementary Material Table S4). Furthermore, they are also enriched in large ion lithophile elements (LILEs) (Rb, Ba and K) and depleted in high-field-strength elements (HFSEs) (Nb, Ta and Ti) in the primitive mantle-normalized trace-element diagrams (Fig. 9a).

4.b.2. Rhyolites of the Kulun Formation

The rhyolites presented in this study have variable compositions with SiO_2 = 65.42–76.22 wt %, Al_2O_3 = 12.47–23.56 wt % and high K_2O (4.18–6.69 wt %), low MgO (0.36–0.44 wt %) and very low Na_2O (0.20–0.39 wt %) contents (online Supplementary Material Table S4). All these rhyolite samples are calc-alkaline, and plot in the field of rhyolite on the total alkali ($K_2O + Na_2O$) versus SiO_2 diagram (TAS; Fig. 5a). Our studied rhyolites show obviously high K_2O/Na_2O ratios (17.16–22.93), and are classified as potassic rhyolites according to the Na_2O versus K_2O diagrams proposed by Foley *et al.* (1987). The potassium-enriched characteristic is also supported by their relatively high Th (13.6–32.5 ppm) and low Co (1.7–2.1 ppm) contents (online Supplementary Material Table S4; Hastie *et al.* 2007). Furthermore, these rhyolite samples show distinctly elevated Al_2O_3 contents (up to 23.56 wt %) and show a strongly peraluminous affinity, with A/CNK values ranging from 2.34 to 2.96 (Fig. 5c). These rhyolite samples are enriched in light rare earth elements (LREEs) and have relatively variable ∑REE

https://doi.org/10.1017/S0016756822000358 Published online by Cambridge University Press

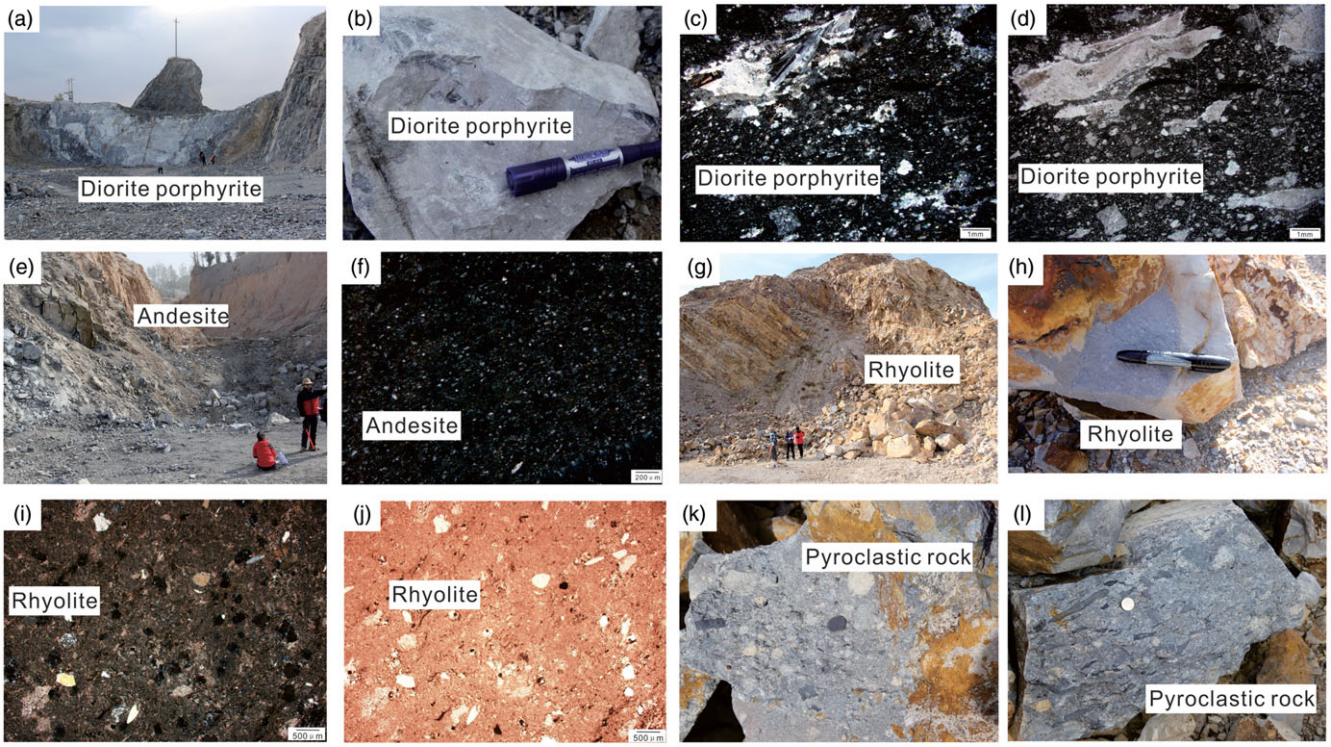

Fig. 4. (Colour online) Representative field outcrops and photomicrographs of the late Palaeozoic magmatic rocks in the Kulun region. Pen for scale is 13.5 cm long. Coin for scale is 2.5 cm diameter.

contents (99.3–332.5 ppm), with $(La/Yb)_N$ ratios and δEu values of 5.66–12.39 and 0.46–0.76, respectively (Fig. 9d). In the primitive mantle-normalized trace-element diagrams, the rhyolite samples show coherent patterns, with depletions in Ba, Nb, Ta, Sr, P and Ti, and enrichments in Rb, Th, U, K, Pb, Zr and Hf (Fig. 9c).

4.b.3. Diorite porphyrites

The analysed diorite porphyrites have $SiO_2 = 56.87–57.91$ wt %, MgO = 1.93–2.11 wt %, $Al_2O_3 = 13.77–13.96$ wt % and $K_2O + Na_2O = 4.85–4.94$ wt %. These rocks show metaluminous affinities, with A/CNK values ranging from 0.39 to 0.42 (Fig. 5c; online Supplementary Material Table S4). In the primitive mantle-normalized patterns, these diorite porphyrite samples are characterized by depletion in HFSEs (e.g. Nb, Ta and Ti) and Ba and Sr, and enrichment in LILEs (e.g. Rb, Th, U and K; Fig. 9a), with negative Eu anomalies (δEu = 0.61–0.65; Fig. 9b).

5. Discussion

5.a. Petrogenesis of the early–middle Permian magmatic suites in the Kulun region

On the basis of petrographic and geochemical studies, the studied early Permian magmatic suites in the Kulun region may be divided into two categories: (1) calc-alkaline andesites and diorite porphyrites; and (2) rhyolites with potassic affinity.

5.a.1. Early Permian andesites and diorite porphyrites

Several models have been proposed to explain the petrogenesis of andesites and diorite porphyrites, including: (1) partial melting of mantle wedge peridotites metasomatized by subduction-related fluids or/and melts (Deng *et al.* 2010); (2) fractional crystallization of mantle-derived basaltic magmas (Maury *et al.* 1978; Zhang, J. H. *et al.* 2010); (3) mixing of mantle- and crust-derived magmas or crustal contamination processes (Cantagrel *et al.* 1984); and (4) partial melting of mafic lower crust (Jung *et al.* 2002).

The early Permian andesites and diorite porphyrites investigated in this study contain high SiO_2 and total alkali ($Na_2O + K_2O$) contents, with prominently low contents of MgO and transition metal elements (e.g. Cr, Co and Ni) and Mg no. values, indicating that their primitive magmas were unlikely to directly generate by partial melting of primitive mantle (Sun & McDonough, 1989). This is because that partial melting of such mantle sources at a diverse range of pressures and degrees of partial melting might only generate mafic to high-Mg intermediate melts (Hofmann, 1988). Furthermore, if these andesites and diorite porphyrites presented in this study were formed through fractional crystallization of mantle-derived basaltic magmas, then the volume of the exposed basaltic materials in the Kulun region would greatly exceed that of the intermediate rocks; however, this is not the case. Based on the relatively narrow ranges of concentrations of TiO_2 (0.64–0.97 wt %), MgO (1.44–2.11 wt %) and $Fe_2O_3^T$ (4.36–5.99 wt %), the small plotting areas (TAS diagram; Fig. 5a) and the lack of significantly negative Eu anomalies (δEu = 0.61–0.76), fractional crystallization did not play a crucial role during their petrogenesis. Mixing between mantle- and crust-derived magmas or crustal contamination processes could explain the origin of the andesites and diorite porphyrites. Captured zircon from the andesites and diorite porphyrites could support this model. The mixing hypothesis was excluded, however, based on the following evidence: (1) mafic microgranular enclaves and chemical variations resulted from mixing mechanisms are absent; (2) on the La/Sm versus SiO_2 and Th/La versus SiO_2 plots, the SiO_2 contents show no correlation with La/Sm or Th/La ratios, indicating that crustal

https://doi.org/10.1017/S0016756822000358 Published online by Cambridge University Press

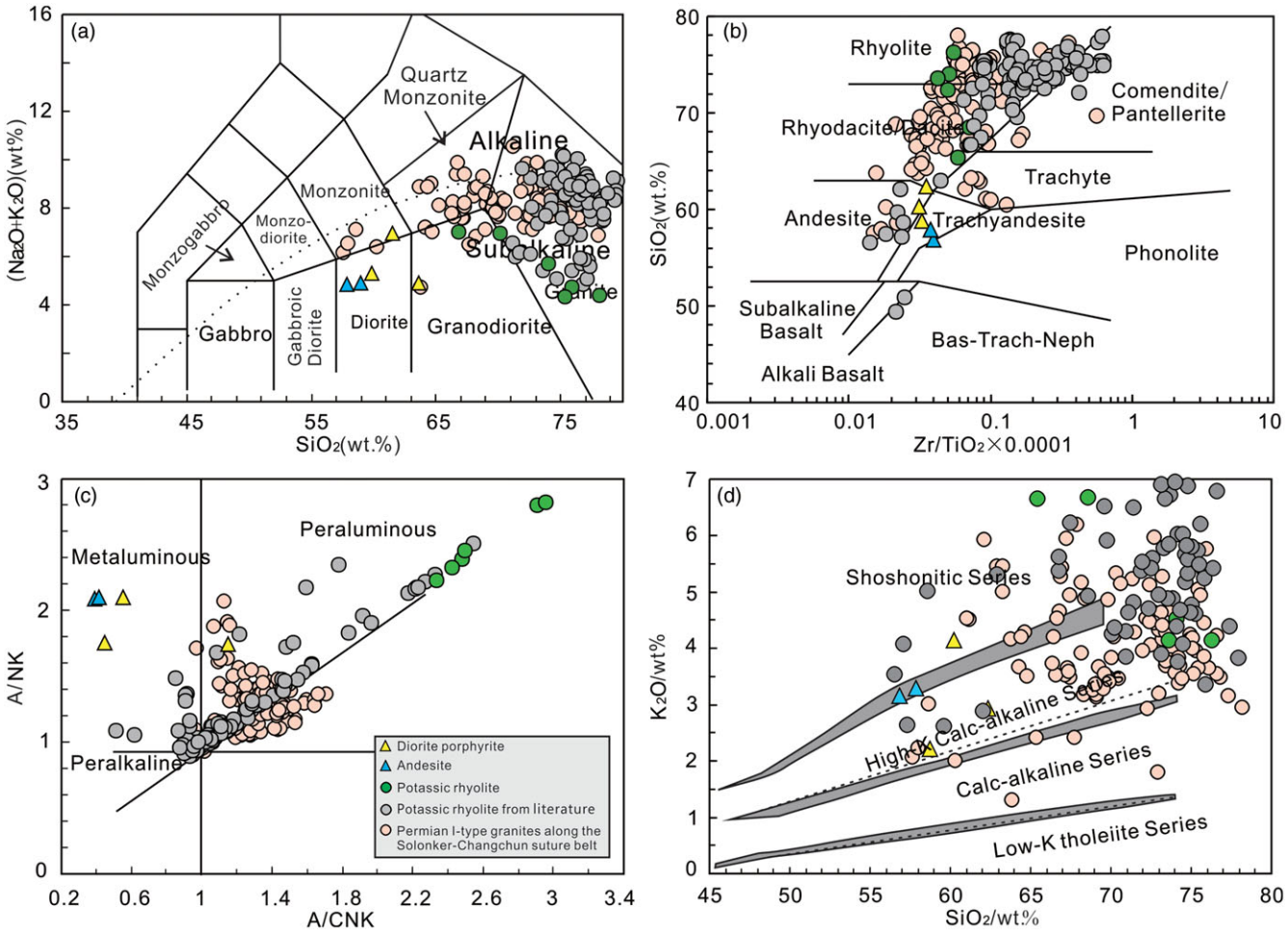

Fig. 5. (Colour online) Plots of (a) total alkali versus SiO_2 diagram (TAS, Peccerillo & Taylor, 1976); (b) SiO_2 versus Zr/TiO_2 *0.0001 (Winchester & Floyd, 1977); (c) A/NK (molar ratio $Al_2O_3/(Na_2O + K_2O)$) versus A/CNK (molar ratio $Al_2O_3/(CaO + Na_2O + K_2O)$) (Maniar & Piccoli, 1989); (d) K_2O versus SiO_2 (Peccerillo & Taylor, 1976) for the late Palaeozoic magmatic rocks in the Kulun region along the Solonker–Changchun suture zone. The data for Permian granites along the Solonker–Changchun suture zone are from Jing *et al.* (2020*a*,*b* and references therein). Typical potassic rhyolite data are from Samuel *et al.* (2007), Hu *et al.* (2013), Ding *et al.* (2015) and Chen *et al.* (2016).

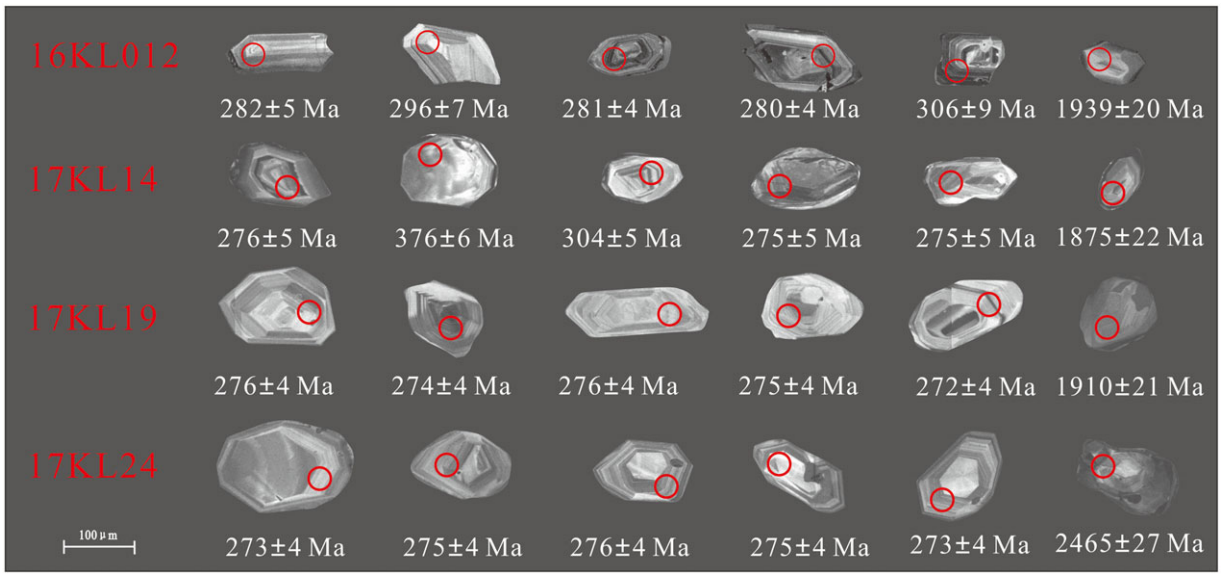

Fig. 6. (Colour online) Cathodoluminescence (CL) images of zircons from the late Palaeozoic magmatic rocks in the Kulun region, with U–Pb analytical spots indicated by red circles.

https://doi.org/10.1017/S0016756822000358 Published online by Cambridge University Press

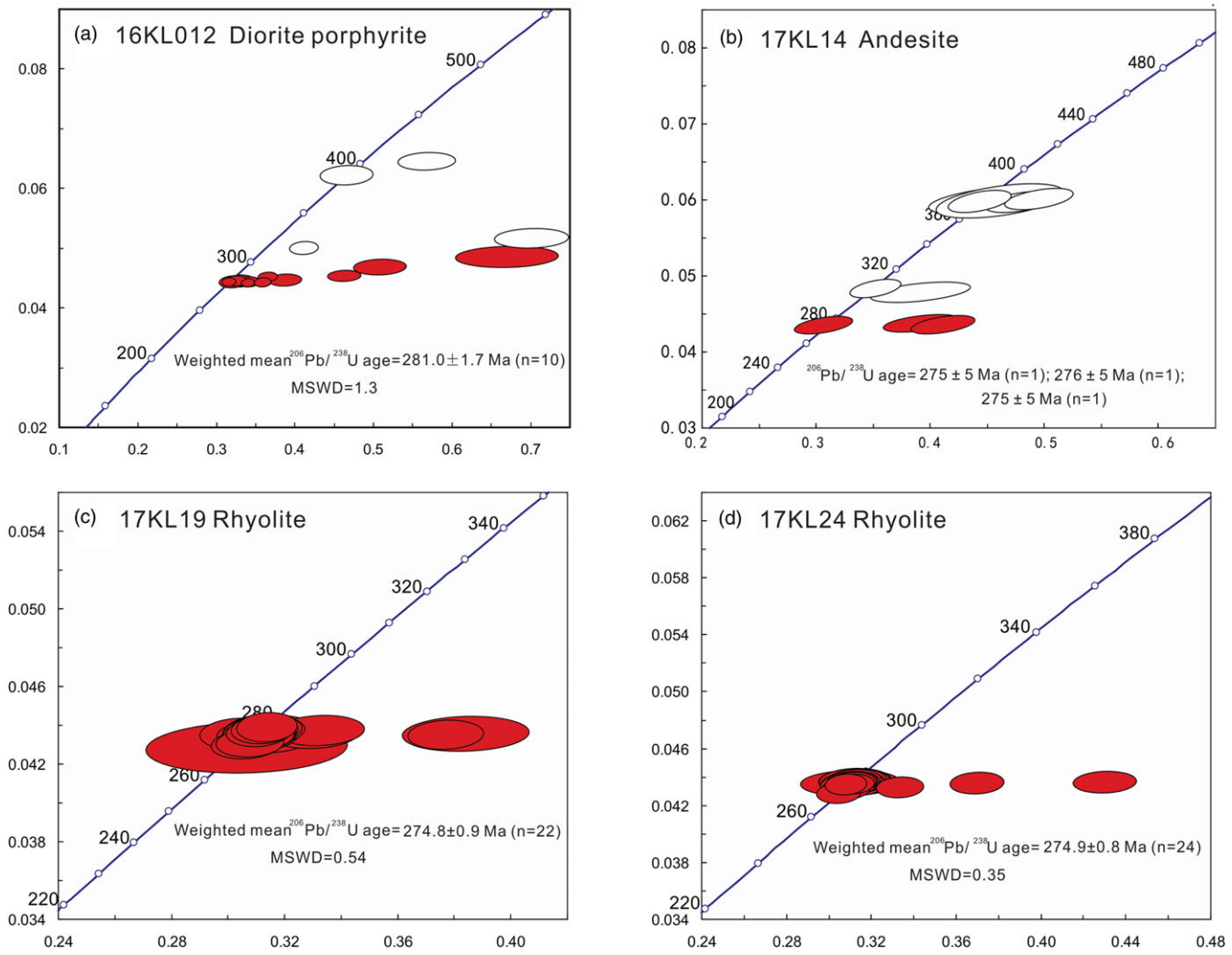

Fig. 7. (Colour online) U–Pb concordia diagrams showing zircon ages obtained by LA-ICP-MS for the late Palaeozoic magmatic rocks in the Kulun region, with weighted mean ages and MSWD shown in each figure. The red ellipses represent age points which are used for the calculation of weighted mean age, whereas the white ellipses represent age points for captured zircons.

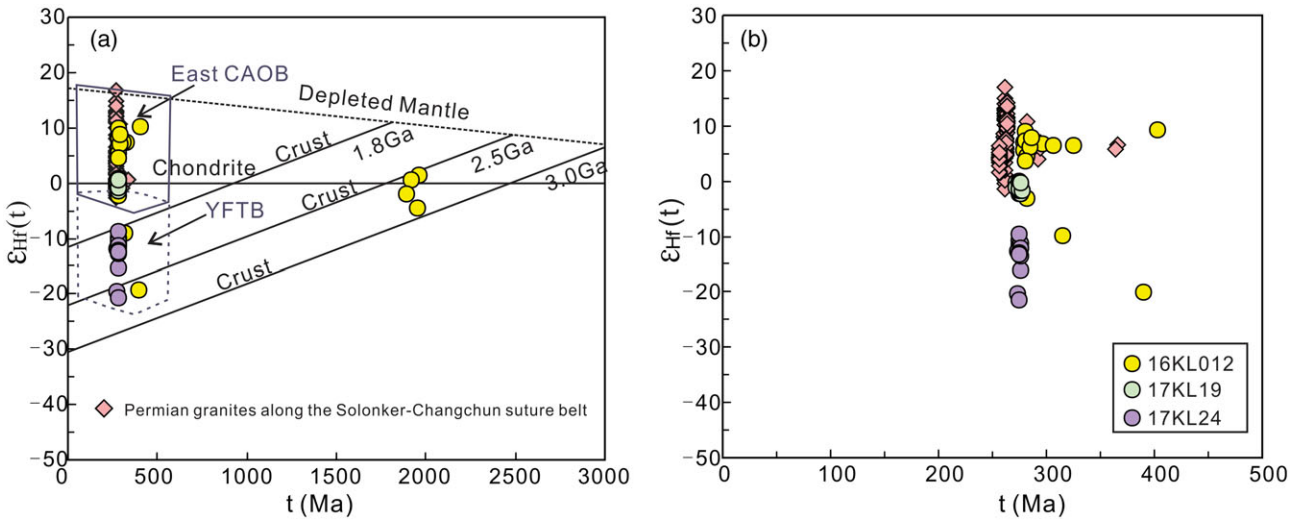

Fig. 8. (Colour online) (a) $\epsilon_{Hf}(t)$ versus T (Ma) diagram for zircons from the late Palaeozoic magmatic rocks in the Kulun region. CAOB – Central Asian Orogenic Belt; YFTB – Yanshan Fold-and-Thrust Belt (Yang *et al.* 2006). (b) Detailed distribution of samples on $\epsilon_{Hf}(t)$ versus T (Ma) diagram. Hf isotopic data for the Permian granites along the Solonker–Changchun suture zone are from Jing *et al.* (2020*a*,*b* and references therein).

https://doi.org/10.1017/S0016756822000358 Published online by Cambridge University Press

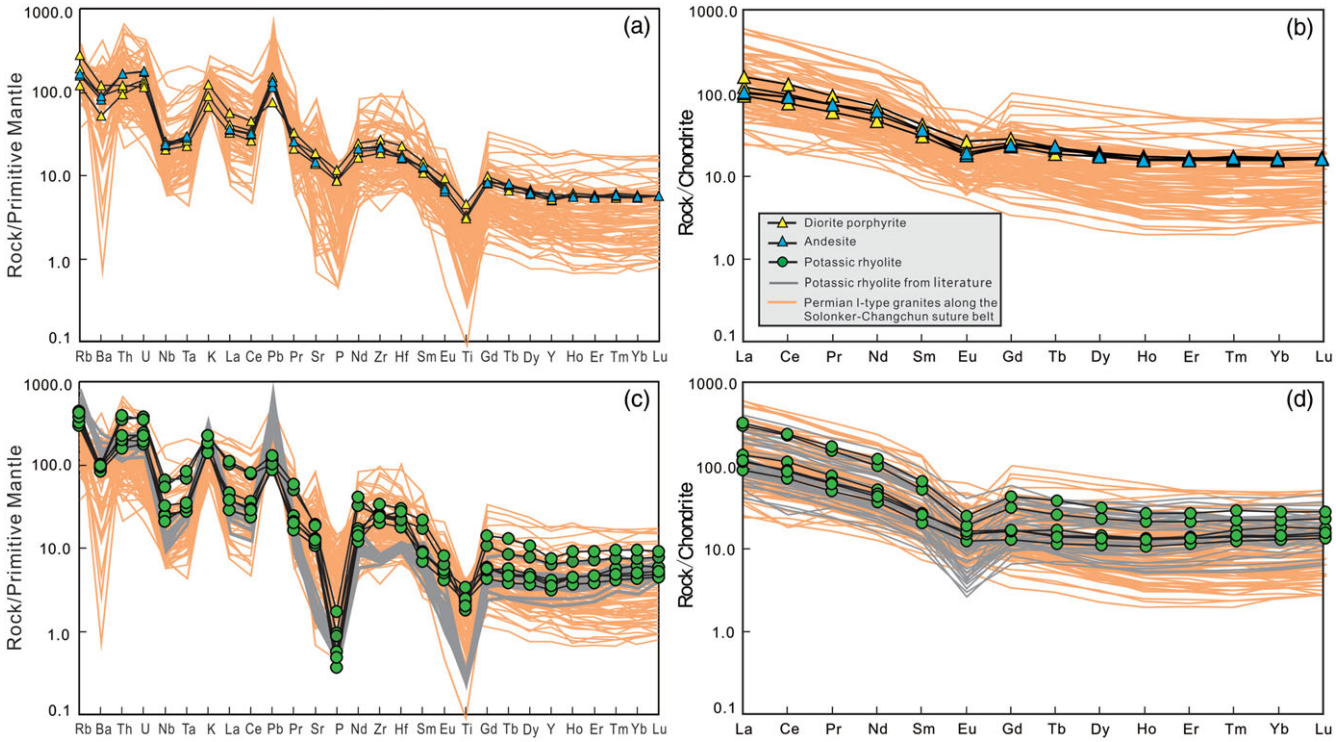

Fig. 9. (Colour online) (a, c) Primitive mantle-normalized trace-element patterns and (b, d) chondrite-normalized REE patterns for the late Palaeozoic magmatic rocks in the Kulun region along the Solonker–Changchun suture zone. Primitive mantle-normalized and chondrite-normalized values are from Sun & McDonough (1989). The data for Permian granites along the Solonker–Changchun suture zone are from Jing *et al.* (2020*a*,*b* and references therein). Typical potassic rhyolite data are from Samuel *et al.* (2007), Hu *et al.* (2013), Ding *et al.* (2015) and Chen *et al.* (2016).

contamination was limited during the magmatic evolution (online Supplementary Material Fig. S1); and (3) Zr and Hf, which are typically enriched during crustal contamination, are absent. The minor contamination indicated by the captured zircons might be explained by the mixing of zircons concentrated in some sedimentary rocks.

We consider that the last model based on partial melting of mafic lower crustal materials best reflects the petrogenesis of the andesites and diorite porphyrites. As mentioned above, the rocks are classified as high-K to medium-K calc-alkaline series, and characterized by enrichments in LREEs and LILEs, and depletions in HFSEs and heavy rare earth elements (HREEs). Their low MgO contents, Mg no. values, low Cr and Ni concentrations, together with similar REE and trace-element patterns to those of bulk continental crust, thus exhibit a crustal affinity (Fig. 9a, b; Rudnick & Gao, 2003). Furthermore, the Rb/Sr, Ti/Y and Ti/Zr ratios of these rocks vary from 0.26 to 0.46, 141.19 to 248.14, and 15.13 to 19.33, respectively, and all these ratios are representative of crustal values, implying that their primitive magmas were originated from the partial melting of lower crustal materials (Rudnick, 1995; Sun & McDonough, 1989). The andesites and diorite porphyrites have relatively high HREEs (Y > 22.9 ppm), which together with their relatively flat HREE patterns (Fig. 9b), preclude the presence of garnet as a residual phase in their source. They also have relatively low Sr contents of <400 ppm (292.4–390.4 ppm), elevated Yb contents (2.6–2.9 ppm) and weakly negative Eu anomalies (0.61–0.76), suggesting an affinity with low-Sr and high-Yb type rocks as defined by Zhang *et al.* (2006). These characteristics, together with their weak concave-upward shape of middle REEs and negative Eu anomalies (Fig. 9a, b), indicate amphibolite as a residual facies in the magma source. Experimental petrology has shown that if hornblende is the main residual phase, the corresponding temperature and pressure conditions during partial melting are 10~12.5 kbar and 800~950 °C (i.e. crustal depth is 30~40 km). Thus, the generation of intermediate igneous rocks in the Kulun region requires relatively low-pressure partial melting of amphibolitic lower crust at a crustal depth of 30–40 km (Qian & Hermann, 2013). Furthermore, zircons from the andesites and diorite porphyrites show heterogeneous *in situ* zircon Hf isotopic compositions, with $\epsilon_{Hf}(t)$ values and T_{DM2} ages ranging from –2.6 to +9.7, and 1466 to 684 Ma, respectively, indicating the partial melting of mixed sources of juvenile crust and recycled ancient Meso-Neoproterozoic crustal materials of the NCC (Fig. 8a, b; Yang *et al.* 2006).

5.a.2. Rhyolites with potassic affinity

The rhyolite samples presented in this study from the Kulun region are characterized by high SiO_2 (65.42–76.22 wt %), K_2O (4.18–6.69 wt %) and Al_2O_3 (12.47–23.56 wt %) contents, low MgO (0.36–0.44 wt %) and very low Na_2O (0.20–0.39 wt %) contents, with K_2O/Na_2O ratios of 17.16–22.93. These rhyolites could further be classified as potassic group with $K_2O/Na_2O > 2$ according to the Na_2O versus K_2O diagrams presented in Foley *et al.* (1987). However, typical ultrapotassic rocks defined in Foley *et al.* (1987) should have shown high K_2O (>3 wt %), MgO contents >3 wt % and $K_2O/Na_2O > 2$ for whole-rock analyses, with high Mg no. values. These ultrapotassic rocks retrieved by a literature review carried out by Foley *et al.* (1987) are grouped into three major geochemical end-member groups, including lamproites, kamafugites, and rocks with high CaO and Al_2O_3 occurring in orogen zones (Miller *et al.* 1999; Williams *et al.* 2004; Liu *et al.* 2014). The third group of rocks have low Mg no. due to fractional

https://doi.org/10.1017/S0016756822000358 Published online by Cambridge University Press

crystallization, but their primary magmas also show characteristics of mantle derivation. These ultrapotassic magmatic rocks, such as lamprophyre dykes presented in Liu, Z. C. *et al.* (2020) are important indicators for extensional tectonic environments, such as post-collisional extension, continental rift, and intraplate rift.

However, elevated SiO_2 and total alkali ($Na_2O + K_2O$), low MgO, and transition metal element (e.g. Cr, Co and Ni) contents, enrichments in LREEs, high positive Zr–Hf anomalies and depletions in Nb and Ta preclude a primitive mantle origin (Rudnick, 1995). We argue that these rhyolite samples may be a result of partial melting of crustal materials. Our conclusion is based on the following evidence. Firstly, zircons from intermediate igneous rocks show heterogeneous Hf isotopic compositions, with $\epsilon_{Hf}(t)$ values and T_{DM2} ages ranging from −2.6 to +9.7, and 1466 to 684 Ma, respectively. However, zircons from the rhyolite samples show wide variations in Hf isotopic data, with $\epsilon_{Hf}(t)$ values and T_{DM2} ages of −20.8 to +0.5 and 3578~1494 Ma, respectively. Since radiogenic isotopic compositions are not changed by partial melting or fractional crystallization of magma, thus they can be used to trace the nature of the mantle source. The rhyolite samples have obvious negative $\epsilon_{Hf}(t)$ values, implying that their magma source might contain more ancient crustal materials of the NCC. Then, the absence of voluminous coeval basaltic or andesitic materials within the Kulun region precluded the possibility of extensive fractional crystallization model. In addition, the rhyolite samples in the Kulun region show high Th and U contents (13.6–32.5 ppm and 3.8–7.7 ppm, respectively), high Th/Ce ratios (0.21–0.36) and low Eu/Eu* ratios (<1) that are comparable with upper crustal values (Rudnick & Fountain, 1995; Rudnick & Gao, 2003). Together with their trace-element and REE patterns that are similar to those of upper crust, we suggest that these rhyolites were derived from the partial melting of upper crust (Kerrich *et al.* 1999). All the evidence indicates that the magma source of the studied rhyolites is dominated by Archaean–Mesoproterozoic ancient crustal components with minor juvenile crustal contributions.

Therefore we turn our attention to the most striking features of these rhyolite samples in the Kulun region, that is strong Na depletions and relative K enrichments, and resultant high K_2O/Na_2O ratios (17.16–22.93). To date, several hypotheses have been proposed to explain the K_2O enrichments and Na_2O depletions for the potassic affinity, including weathering, geochemical alteration, fractional crystallization and high-temperature K-metasomatism (McLennan, 1993; Ennis *et al.* 2000).

The rhyolite samples in the Kulun region investigated in this study have relatively low loss on ignition values (mean = 2.21 wt %). These rhyolites still retain their primary magmatic texture, structure and mineral associations, even though weak mineral alteration of sericitization and kaolinitization has occurred (Fig. 4g, j). Furthermore, Th is considered as being immobile during low-grade alteration of igneous rocks; thus, it has been employed to monitor other trace elements (Gibson *et al.* 1982). Analyses show that SiO_2, MgO, P_2O_5 Al_2O_3, almost all of REEs, Nb, Ta, Ti, Zr, and Hf correlate well with Th (online Supplementary Material Table S4), implying their relative immobilities. In addition, K_2O, Rb, Sr and Ba also display good correlations with Th (online Supplementary Material Table S4), further excluding the influence of geochemical alteration during post-eruption processes.

Available studies have shown that high-temperature K-metasomatism can result in the formation of magmas with potassic affinity, which are characterized by increased K_2O, Rb, and Zn contents, a decrease in Na_2O contents, as well as depletions in REEs (Kinnaird *et al.* 1985). The analysed rhyolites, however, have Rb contents ranging from 188.2 to 277.8 ppm, clearly lower than those of rhyolites with potassic characteristics resulting from K-metasomatism (≥1000 ppm; Samuel *et al.* 2007). All these characteristics do not support a model of high-temperature K-metasomatism. Previous studies have also shown that the fractional crystallization of plagioclase could account for the generation of potassic magmas (Shan *et al.* 2007). These rhyolites with potassic affinity from the Kulun region show variations in major and trace elements and have negative anomalies of Ba, Sr and Eu (0.46–0.76), indicating that the primary magma had undergone a certain degree of fractional crystallization. The positive correlations between Sr and Ba and δEu versus Ba, together with negative correlations between Sr versus SiO_2 (online Supplementary Material Table S4), further suggested that the fractional crystallization indeed occurred during genetic evolution, as plagioclase is enriched in Eu and Sr (Fig. 10a–d; Rapp *et al.* 2003). However, in consideration of the obviously low Rb/Sr ratios (0.66–0.91) for these rhyolites, the removal of plagioclase from the felsic magmas was minor and consequently had a limited effect on the very low Na_2O contents (Ajaji *et al.* 1998).

Experimental investigations have further demonstrated that the processes of liquid immiscibility of the felsic magmas also contributed to the potassium-rich affinity, as Na_2O dissolves more favourably than K_2O in the volatiles during the magmatic evolution in the magma chamber (Veksler & Thomas, 2002; Veksler, 2004; Samuel *et al.* 2007). The explosive eruption of volcanoes with a high volatile content naturally causes the removal of a great part of Na_2O in melts, as well as K_2O contents to a lesser degree (Samuel *et al.* 2007). It is noteworthy that most reported potassic or/and ultrapotassic rhyolites are always associated with abundant pyroclastic rocks in the field outcrops (Fig. 4k, l); examples are the Wadi El-Mahash and Gebel El-Homra ultrapotassic rhyolites in Sinai (Samuel *et al.* 2007), the Tanggula Pass ultrapotassic rhyolites in southern Qiangtang (Chen *et al.* 2016), and the Lhasa ultrapotassic rhyolites in southern Tibet (Ding *et al.* 2015). These characteristics suggest a crucial role for the accumulation of gases, vapours or volatiles. In this case, the remaining alumina would import more potassium into the magma chamber, forming more alkaline feldspars owing to the lack of sodium, as well as the increase in normative corundum content. Based on a calculation of the CIPW norms, these rhyolites in the Kulun region with potassic affinity presented in this study have high contents of normative corundum, further supporting this hypothesis. Calculation results show that these rhyolite samples from the Kulun region have normative corundum values ranging from 5.35 to 11.18 vol. % and 7.49 to 15.70 wt %, respectively. Therefore the potassic affinity of these rhyolites from the Kulun region is dominantly ascribed to liquid immiscibility of felsic magma, as subsequent fractional crystallization and removal of plagioclase were limited.

5.b. The late Palaeozoic geodynamic evolution of the eastern Palaeo-Asian Ocean

The Solonker–Changchun suture zone has been considered as the locus for the final disappearance of the eastern Palaeo-Asian Ocean between the NCC and the northern micro-continental blocks (combined NE China blocks; Sengör *et al.* 1993; Badarch *et al.* 2002; Li, 2006; Zhou, J. B. *et al.* 2010, 2018; Wilde, 2015; Eizenhöfer & Zhao, 2018; Chai *et al.* 2020). However, the proposed hypotheses favoured that the suturing took place in the Middle Devonian to Carboniferous (Tang, 1990; Xu *et al.* 2013, 2015; Zhao *et al.* 2013, 2020), early

https://doi.org/10.1017/S0016756822000358 Published online by Cambridge University Press

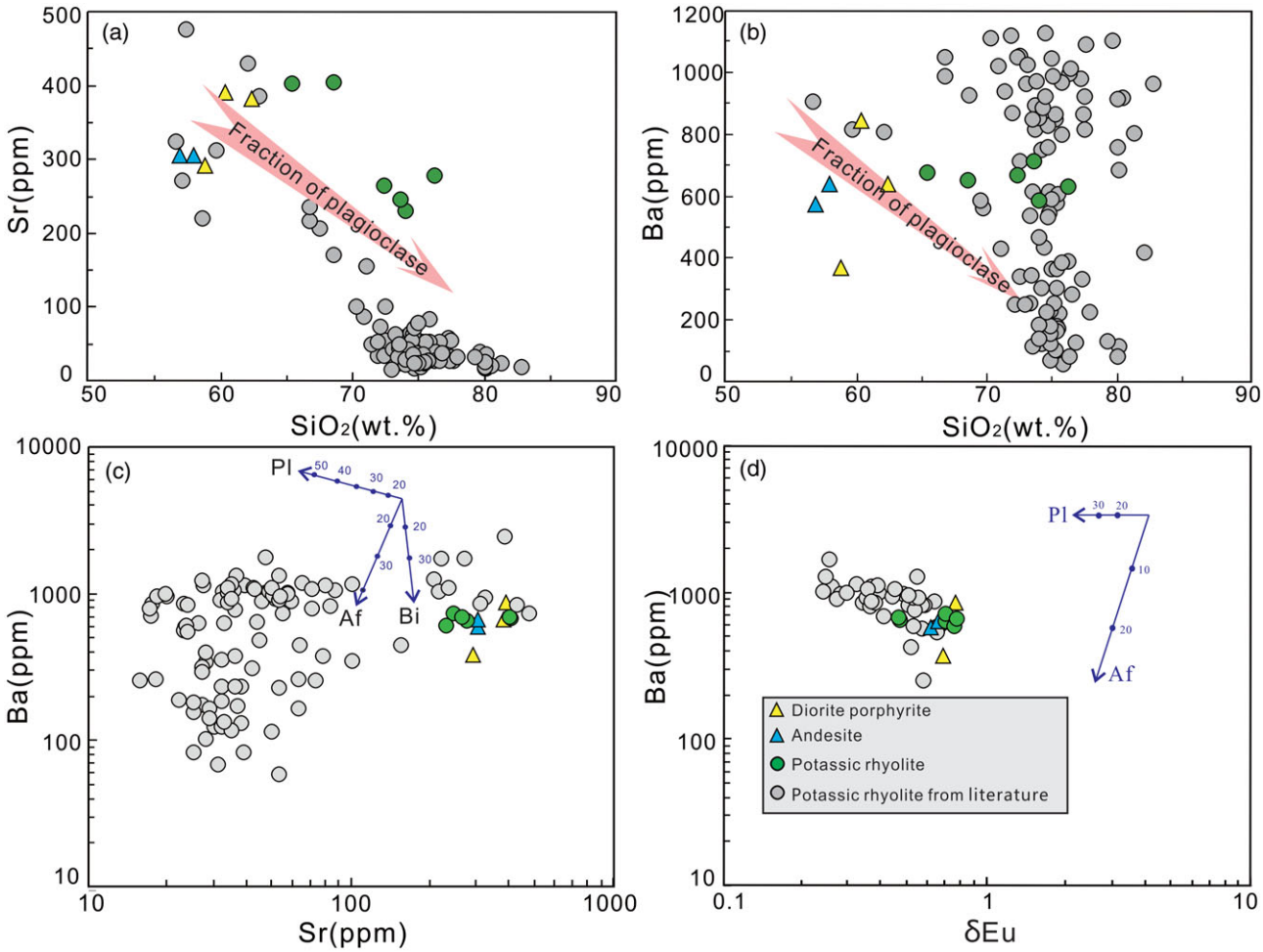

Fig. 10. (Colour online) Diagrams of (a) Sr versus SiO_2, (b) Ba versus SiO_2, (c) Ba versus Sr, and (d) Ba versus δEu for the late Palaeozoic magmatic rocks in the Kulun region along the Solonker–Changchun suture zone. Typical potassic rhyolite data are from Samuel *et al.* (2007), Hu *et al.* (2013), Ding *et al.* (2015) and Chen *et al.* (2016).

Permian (Zhang *et al.* 2012) or late Permian–Middle Triassic (Sengör *et al.* 1993; Xiao *et al.* 2003, 2015; Yu *et al.* 2014; Eizenhöfer *et al.* 2014; Wilde, 2015; Yuan *et al.* 2016; Guo *et al.* 2016; Liu, J. *et al.* 2016, 2020; Huang *et al.* 2018; Eizenhöfer & Zhao, 2018; Song *et al.* 2018; Jing *et al.* 2020*a*,*b*; Chai *et al.* 2020) periods. Important insights into the tectonic evolution of the eastern CAOB, which formed in response to the subduction, accretion and final closure of the Palaeo-Asian Ocean, are provided by the early Permian magmatic rocks in the Kulun region (Cao *et al.* 2013; Xu *et al.* 2013, 2015; Yu *et al.* 2014; Wilde, 2015; Xiao *et al.* 2015; Liu, J. *et al.* 2016, 2020; Song *et al.* 2018; Jing *et al.* 2020*a*; Chai *et al.* 2020).

The early Permian igneous rocks in the Kulun region are predominantly andesites, rhyolites, and diorite porphyrites. They belong to the high-K calc-alkaline to shoshonite series, and show enrichments in LREEs and LILEs, and depletions in HREEs (Nb, Ta and Ti) and HFSEs. These geochemical characteristics are similar to the volcanic rocks formed in an active continental margin environment analogous to the modern Andes (Pearce, 1982; Pitcher, 1983; Xiao *et al.* 2003). Furthermore, Th/Ta ratios have been used to discriminate active continental margins from oceanic arcs based on immobile elements (Gorton & Schandl, 2000). These studied intermediate-acidic volcanic rocks have relatively high Th/Ta ratios and display an affinity with active continental margins (Fig. 11a). The same conclusion is also verified in the Hf–(Rb/30)–(Ta*3) discrimination diagram, as most intermediate-acidic volcanic rock samples from the Kulun region plot into the area of volcanic arc granites (VAG; Fig. 11b). These results, combined with previously published data, identify an E–W-trending calc-alkaline magmatic belt from early Carboniferous to Early Triassic times (347–250 Ma) along the Solonker–Changchun suture zone (Li, 2006; Wu *et al.* 2011; Li *et al.* 2014, 2016; Guo *et al.* 2016; Yuan *et al.* 2016; Song *et al.* 2018; Liu, J. *et al.* 2020; Jing *et al.* 2020*a*,*b*). The magmatic belt was believed to be the product of the Andean-type active continental margin environments in response to southward subduction of the eastern Palaeo-Asian Ocean (Fig. 1b; Li, 2006; Zhou *et al.* 2010; Wu *et al.* 2011; Wilde, 2015; Eizenhöfer & Zhao, 2018; Zhou, Z. B. *et al.* 2018). Magmatic activities were prolonged, lasting for ~100 Myr from 347 Ma to 250 Ma, and cannot be related to continental rifting or a post-collision extension, but is coincident with the subduction-related arc magmatism caused by the southward subduction of the eastern Palaeo-Asian Ocean slab (Fig. 1b; online Supplementary Material Table S1). High-magnesium andesites with ages of *c.* 250 Ma have been identified recently in the Kaiyuan and Linxi regions along the Solonker–Changchun suture zone, further demonstrating that the eastern Palaeo-Asian Ocean existed until Early Triassic time (Liu *et al.* 2012; Yuan *et al.* 2016).

https://doi.org/10.1017/S0016756822000358 Published online by Cambridge University Press

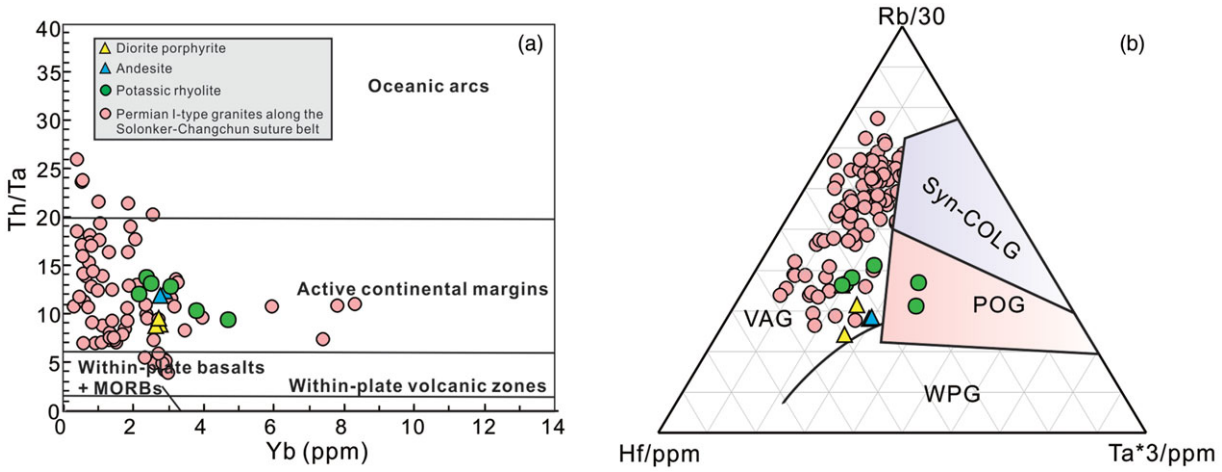

Fig. 11. (Colour online) Diagrams of (a) Th/Ta versus Yb (Gorton & Schandl, 2000), and (b) Hf–(Rb/30)–(Ta*3) ternary variation diagram (Harris *et al.* 1986) for the late Palaeozoic magmatic rocks in the Kulun region along the Solonker–Changchun suture zone. Abbreviations: VAG – volcanic arc granites; WPG – within-plate granites; syn-COLG – syn-collisional granites; POG – post-collisional granites; MORBs – mid-ocean ridge basalts. The data for Permian granites along the Solonker–Changchun suture zone are from Jing *et al.* (2020*a*,*b* and references therein). Typical potassic rhyolite data are from Samuel *et al.* (2007), Hu *et al.* (2013), Ding *et al.* (2015) and Chen *et al.* (2016).

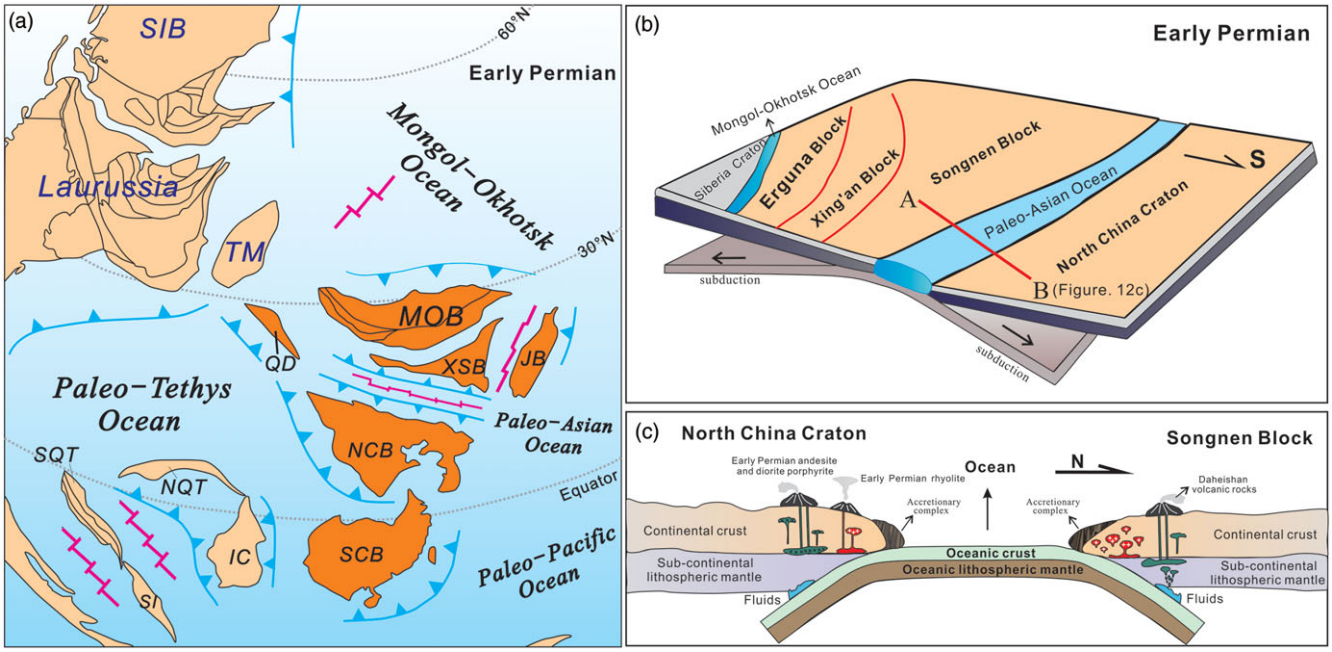

Fig. 12. (Colour online) (a) Palaeogeographic reconstruction model of the East Asian blocks and Gondwana, Laurussia and Siberia during the early Permian period (Ren *et al.* 2020). Abbreviations: NQT – North Qiangtang Terrane; SQT – South Qiangtang Terrane; SI – Sibumasu Block; IC – Indochina Block; SIB – Siberia Block; TM – Tarim Block; QD – Qaidam Block; NCB – North China Block; SCB – South China Block; XSB – Xilinhot–Songliao Block; MOB – Mongolia Block; JB – Jiamusi–Bureya Block. (b) Schematic models for the early Permian tectonic evolution of the eastern Palaeo-Asian Ocean.

In addition, models that propose an Early–Middle Devonian age for the final closure of the eastern Palaeo-Asian Ocean (Xu *et al.* 2013) cannot explain the occurrence of middle Permian radiolarians and conodonts in the northern Solonker–Changchun suture zone (Wang, 1997). The amalgamation of the Angara and Cathaysian floras along the Solonker–Changchun suture zone in late Permian time (Deng *et al.* 2009), and the occurrence of marine pelagic facies in the middle Permian Zhesi Formation and mixed marine-terrestrial facies in the upper Permian Linxi Formation in the southeastern CAOB support a latest Permian–Early Triassic age for the final closure of the eastern Palaeo-Asian Ocean (Shang, 2004). Furthermore, the latest researches on regional metamorphism in the southeastern CAOB carried out by Li *et al.* (2021) revealed a medium-pressure metamorphism in the eastern Songnen Block, and the metamorphic conditions were under lower-amphibolite-facies with *P*–*T* conditions of 5.5–7.1 kbar and 592–630 °C. The medium-pressure metamorphism occurred in late Permian time (260–251 Ma), which was associated with the collision between the combined NE China blocks and the NCC in response to the final closure of the Palaeo-Asian Ocean. We thus support those models advocating the final closure of the eastern Palaeo-Asian Ocean occurring in latest late Permian–Early Triassic times.

https://doi.org/10.1017/S0016756822000358 Published online by Cambridge University Press

Abundant palaeomagnetic data obtained over the past few decades have provided additional constraints on the geodynamic evolution of the eastern Palaeo-Asian Ocean during the Permian–Triassic period. For example, Zhang *et al.* (2018) proposed that the final closure of the eastern Palaeo-Asian Ocean occurred in late Permian–Early Triassic times (*ca.* 250 Ma), as no significant latitudinal difference between the southeastern CAOB blocks was indicated by palaeomagnetic data from Permian volcanic rocks (the Sanmianjing, Elitu and Dashizhai formations) (Huang *et al.* 2018). In addition, Zhang *et al.* (2021) further reported two robust palaeomagnetic results from 320–280 Ma volcanic strata in the South Mongolia–Xing'an Belt, and the results indicate that the northward motion of North China and Mongolia paralleled Laurussia from late Carboniferous–early Permian times. Quantization results show the N–S width of the Palaeo-Asian Ocean in the east-central segment was *ca.* 2700 km during late Carboniferous to early Permian times. It is therefore suggested the early Permian magmatic rocks in the Kulun region were formed in an active continental margin setting influenced by the southward subduction of the eastern Palaeo-Asian Ocean. The widespread occurrence of the latest Early–Middle Triassic syn-collisional granites such as the Dayushan pluton (Sun *et al.* 2004), Dongfeng granite (Xin *et al.* 2011) and Baicaoping porphyrite (Zhang *et al.* 2004) along the Solonker–Changchun suture zone also suggests a prolonged contraction (*Jing et al.* 2022). Thus, we prefer that the eastern Palaeo-Asian Ocean likely closed during Early–Middle Triassic time (Fig. 12; Xiao *et al.* 2003; Li, 2006; Wu *et al.* 2011; Cao *et al.* 2013; Eizenhöfer *et al.* 2014; Li *et al.* 2014, 2016; Wilde, 2015; Yuan *et al.* 2016; Huang *et al.* 2018; Song *et al.* 2018; Eizenhöfer & Zhao, 2018; Liu, J. *et al.* 2020; Jing *et al.* 2020*a*,*b*; Zhao *et al.* 2020).

6. Conclusions

Based on geochronological and geochemical studies, early Permian arc magmatic suites with a crystallization age of *ca.* 275 Ma have been identified in the Kulun region of the southeastern CAOB. The diorite porphyrites and andesites show crustal affinities and originated by partial melting of amphibolitic lower crust at a crustal depth of 30–40 km. The rhyolites show potassic affinity and heterogeneous zircon Hf isotopic signatures, with predominately negative values. These characteristics suggest a mixed source dominated by recycled older crust mixed with minor juvenile crustal materials. The potassic affinity of these rhyolites from the Kulun region is dominantly ascribed to liquid immiscibility of felsic magma, as subsequent fractional crystallization and removal of plagioclase were limited. Identification of this early Permian magmatic association and coeval arc-style magmatic rocks provides evidence of an active continental margin linked to the southward subduction of the Palaeo-Asian oceanic slab.

Supplementary material. To view supplementary material for this article, please visit https://doi.org/10.1017/S0016756822000358

Acknowledgements. We appreciate the staff (Li Su, Yu-jie Hao and Wen-qing Li) of China University of Geosciences (Beijing) and Jilin University for their support and help during the analyses of U–Pb isotopes. We are sincerely grateful to the staff (Jun-hui Bi and Hong-ying Zhou) of the Institute of Geology and Mineral Resources in Tianjin, because of their help, support and care during the process of the zircon Hf isotopic analyses. We also appreciate Sarah Sherlock for helpful comments in his handling of this manuscript, and we thank two anonymous reviewers for their detailed, constructive comments that have greatly improved the manuscript. This manuscript is subsidized by the National Natural Science Foundation of China (41872056).

References

Ajaji T, Weis D, Giret A and Bouabdellah M (1998) Coeval potassic and sodic calc-alkaline series in the post-collisional Hercynian Tanncherfi intrusive complex, northeastern Morocco: geochemical, isotopic and geochronological evidence. *Lithos* **45**, 371–93.

Annen C, Blundy JD and Sparks RSJ (2006) The genesis of intermediate and silicic magmas in deep crustal hot zones. *Journal of Petrology* **47**, 505–39.

Badarch G, Cunningham WD and Windley BF (2002) A new terrane subdivision for Mongolia: implications for the Phanerozoic crustal growth of Central Asia. *Journal of Asian Earth Sciences* **21**, 87–110.

Bao ZW, Chen SH and Zhang ZT (1994) A study on REE and Sm–Nd isotopes of Hegenshan ophiolite, Inner Mongolia. *Geochemica* **23**, 339–49 (in Chinese with English abstract).

Cantagrel JM, Didier J and Gourgaud A (1984) Magma mixing: origin of intermediate rocks and "enclaves" from volcanism to plutonism. *Physics of the Earth and Planetary Interiors* **35**, 63–76.

Cao HH, Xu WL, Pei FP, Wang ZW, Wang F and Wang ZJ (2013) Zircon U–Pb geochronology and petrogenesis of the Late Paleozoic–Early Mesozoic intrusive rocks in the eastern segment of the northern margin of the North China Block. *Lithos* **170–171**, 191–207.

Cao HH, Xu WL, Pei FP and Zhang XZ (2011) Permian tectonic evolution in Southwestern Khanka Massif: evidence from zircon U–Pb chronology, Hf isotope and geochemistry of gabbro and diorite. *Acta Geologica Sinica (English Edition)* **85**, 1390–402.

Cawood PA, Wang Y, Xu Y and Zhao G (2013) Locating South China in Rodinia and Gondwana: a fragment of greater India lithosphere? *Geology* **41**, 903–6.

Chai H, Ma YF, Santosh M, Hao SL, Luo TW, Fan DQ, Gao B, Zong LB, Mao H and Wang QF (2020) Late Carboniferous to Early Permian oceanic subduction in central Inner Mongolia and its correlation with the tectonic evolution of the southeastern Central Asian Orogenic Belt. *Gondwana Research* **84**, 245–59.

Chen SS, Shi RD, Fan WM, Zou HB, Liu DL, Huang QS, Gong XH, Yi GD and Wu K (2016) Middle Triassic ultrapotassic rhyolites from the Tanggula Pass, southern Qiangtang, China: a previously unrecognized stage of silicic magmatism. *Lithos* **264**, 258–76.

Deng JF, Liu C, Feng YF, Xiao QH, Su SG, Zhao GC, Kong WQ and Cao WY (2010) High magnesian andesitic/dioritic rocks (HMA) and magnesian andesitic/dioritic rocks (MA): two igneous rock types related to oceanic subduction. *Geology in China* **37**, 1112–18 (in Chinese with English abstract).

Deng SH, Wan CB and Yang JG (2009) Discovery of a Late Permian Angara-Cathaysia mixed flora from Acheng of Heilongjiang, China, with discussions on the closure of the Paleoasian Ocean. *Science in China (Series D: Earth Sciences)* **52**, 1746–55.

Ding HX, Zhang ZM, Dong X, Yan R, Lin YH and Jiang HY (2015) Cambrian ultrapotassic rhyolites from the Lhasa terrane, south Tibet: evidence for Andean-type magmatism along the northern active margin of Gondwana. *Gondwana Research* **27**, 1616–29.

Dong Y, Ge WC, Yang H, Ji Z, He Y, Zhao D and Xu WL (2018) Convergence history of the Jiamusi and Songnen-Zhangguangcai Range massifs: insights from detrital zircon U–Pb geochronology of the Yilan Heilongjiang Complex, NE China. *Gondwana Research* **56**, 51–68.

Eizenhöfer PR and Zhao GC (2018) Solonker Suture in East Asia and its bearing on the final closure of the eastern segment of the Palaeo-Asian Ocean. *Earth-Science Reviews* **186**, 153–72.

Eizenhöfer PR, Zhao GC, Zhang J and Sun M (2014) Final closure of the Paleo-Asian Ocean along the Solonker Suture Zone: constraints from geochronological and geochemical data of Permian volcanic and sedimentary rocks. *Tectonics* **33**, 441–63.

Ennis DJ, Dunbar NW, Campbell AR and Chapin CE (2000) The effects of K-metasomatism on the mineralogy and geochemistry of silicic ignimbrites near Socorro, New Mexico. *Chemical Geology* **167**, 285–312.

Foley SF, Venturelli G, Green DH and Toscani L (1987) The ultrapotassic rocks: characteristics, classification, and constraints for petrogenetic models. *Earth-Science Reviews* **24**, 81–134.

Ge WC, Wu FY, Zhou CY and Zhang JH (2005) Zircon U–Pb ages and its significance of the Mesozoic granites in the Wulanhaote region, central Da Hinggan Mountain. *Acta Petrologica Sinica* **21**, 749–62 (in Chinese with English abstract).

Gibson SA, Kirkpatrick RJ, Emmermann R, Schmincke H-U, Pritchard G, Oakley PJ, Thorpe RS and Marriner GF (1982) The trace element composition of lavas and dikes from a 3-km vertical section through a lava pile in eastern Iceland. *Journal of Geophysical Research: Solid Earth* **87**, 6532–46.

Gorton MP and Schandl ES (2000) From continents to island arcs: a geochemical index of tectonic setting for arc-related and within-plate felsic to intermediate volcanic rocks. *The Canadian Mineralogist* **38**, 1065–73.

Guo F, Li HX, Fan WM, Li JY, Zhao L and Huang MW (2016) Variable sediment flux in generation of Permian subduction-related mafic intrusions from the Yanbian region, NE China. *Lithos* **261**, 195–215.

Harris NBW, Pearce JA and Tindle AG (1986) Geochemical characteristics of collision-zone magmatism. In *Collision Tectonics* (eds MP Coward and AC Ries), pp. 67–81. Geological Society of London, Special Publication no. 19.

Hastie AR, Kerr AC, Pearce JA and Mitchell SF (2007) Classification of altered volcanic island arc rocks using immobile trace elements: development of the Th–Co discrimination diagram. *Journal of Petrology* **48**, 2341–57.

Hofmann AW (1988) Chemical differentiation of the Earth: the relationship between mantle, continental crust, and oceanic crust. *Earth and Planetary Science Letters* **90**, 297–314.

Hu PY, Li C, Wang M, Xie C and Wu YW (2013) Cambrian volcanism in the Lhasa terrane, southern Tibet: record of an early Paleozoic Andean-type magmatic arc along the Gondwana proto-Tethyan margin. *Journal of Asian Earth Sciences* **77**, 91–107.

Huang BC, Yan YG, Piper JDA, Zhang DH, Yi ZY, Yu S and Zhou TH (2018) Paleomagnetic constraints on the paleogeography of the East Asian blocks during Late Paleozoic and Early Mesozoic times. *Earth-Science Reviews* **186**, 8–36.

Hui J, Zhang KJ, Zhang J, Qu JF, Zhang BH, Zhao H and Niu PF (2021) Middle–late Permian high-K adakitic granitoids in the NE Alxa block, northern China: orogenic record following the closure of a Paleo-Asian oceanic branch? *Lithos* **400–401**, 106379. doi: 10.1016/j.lithos.2021.106379.

Imayama T, Koh Y, Aoki K, Saneyoshi M, Yagi K, Aoki S, Terada T, Sawada Y, Ikawa C, Ishigaki S, Toyoda S, Tsogtbaatar K and Mainbayar B (2019) Late Permian to Early Triassic back-arc type volcanism in the southern Mongolia volcano-plutonic belt of the Central Asian Orogenic Belt: implication for timing of the final closure of the Palaeo-Asian Ocean. *Journal of Geodynamics* **131**, 101650. doi: 10.1016/j.jog.2019.101650.

Jahn BM, Wu FY and Chen B (2000) Granitoids of the Central Asian Orogenic Belt and continental growth in the Phanerozoic. *Transactions of the Royal Society of Edinburgh: Earth Sciences* **91**, 181–93.

Jing Y, Ge WC, Dong Y, Yang H, Ji Z, Bi JH, Zhou HY and Xing DH (2020a) Early–Middle Permian southward subduction of the eastern Paleo-Asian Ocean: constraints from geochronology and geochemistry of intermediate-acidic volcanic rocks in the northern margin of the North China Craton. *Lithos* **364–365**, 105491. doi: 10.1016/j.lithos.2020.105491.

Jing Y, Ji Z, Ge WC, Dong Y, Yang H and Bi J (2020b) Middle–late Permian I-type granitoids from the Diaobingshan region in the northern margin of the North China Craton: insight into southward subduction of the Paleo-Asian Ocean. *International Geology Review* **63**, 357–79. doi: 10.1080/00206814.2020.1712556.

Jing Y, Yang H, Ge WC, Dong Y, Ji Z, Bi JH, Zhou HY and Xing DH (2022) When did the final closure occur of the eastern Paleo-Asian Ocean: Constraints from the latest Early-Middle Triassic adakitic granites in the southeastern Central Asian Orogenic Belt. *Gondwana Research* **103**, 146–171.

Jung S, Hoernes S and Mezger K (2002) Synorogenic melting of mafic lower crust: constraints from geochronology, petrology and Sr, Nd, Pb and O isotope geochemistry of quartz diorites (Damara orogen, Namibia). *Contributions to Mineralogy and Petrology* **143**, 551–66.

Kerrich R, Polat A, Wyman APD and Hollings P (1999) Trace element systematics of Mg-, to Fe-tholeiitic basalt suites of the Superior Province: implications for Archean mantle reservoirs and greenstone belt genesis. *Lithos* **46**, 163–87.

Khain EV, Bibikova EV, Salnikova EB, Kröner A, Gibsher AS, Didenko AN, Degtyarev KE and Fedotova AA (2003) The Palaeo-Asian ocean in the Neoproterozoic and early Palaeozoic: new geochronologic data and palaeotectonic reconstructions. *Precambrian Research* **122**, 329–58.

Kinnaird JA, Bowden P, Ixer RA and Odling NWA (1985) Mineralogy, geochemistry and mineralization of the Ririwai complex, northern Nigeria. *Journal of African Earth Sciences* **3**, 185–222.

Koschek G (1993) Origin and significance of the SEM cathodoluminescence from zircon. *Journal of Microscopy* **171**, 223–32.

Lan HY, Li SZ, Guo LL, Li XY, Liu YJ, Liu B, Santosh M, Cao XZ, Zhang R and Wang GZ (2022) Mesozoic deformation of the Nadanhada Terrane (NE China) and its implications on the subduction of the Paleo-Pacific Plate. *Journal of Asian Earth Sciences* **232**, 105166. doi: 10.1016/j.jseaes.2022.105166.

Li HH, Yu JJ, Guo XW and Xu WL (2021) Late Permian medium-pressure metamorphism in the eastern Songnen Massif, eastern Central Asian Orogenic Belt (NE China): implications for the final closure of the Paleo-Asian Ocean. *Journal of Asian Earth Sciences* **215**, 104800. doi: 10.1016/j.jseaes.2021.104800.

Li JY (2006) Permian geodynamic setting of northeast China and adjacent regions: closure of the Paleo-Asian Ocean and subduction of the Paleo-Pacific plate. *Journal of Asian Earth Sciences* **26**, 207–24.

Li S, Wilde SA, He ZJ, Jiang XJ, Liu RY and Zhao L (2014) Triassic sedimentation and postaccretionary crustal evolution along the Solonker suture zone in Inner Mongolia, China. *Tectonics* **33**, 960–81.

Li S, Wilde SA, Wang T, Xiao WJ and Guo QQ (2016) Latest Early Permian granitic magmatism in southern Inner Mongolia, China: implications for the tectonic evolution of the southeastern Central Asian Orogenic Belt. *Gondwana Research* **29**, 168–80.

Liu D, Zhao ZD, Zhu DC, Niu YL, Depaolo DJ, Harrison M, Mo XX, Dong GC, Zhou S, Sun CG, Zhang ZC and Liu JL (2014) Identifying mantle carbonatite metasomatism through Os–Sr–Mg isotopes in Tibetan ultrapotassic rocks. *Geochimica et Cosmochimica Acta* **143**, 207–31.

Liu J, Liu ZH, Li SC, Zhao C, Wang CJ, Peng YB, Yang ZJ and Dou SY (2016) Geochronology and geochemistry of Triassic intrusive rocks in Kaiyuan area of the eastern section of the northern margin of North China. *Acta Petrologica Sinica* **32**, 2739–56 (in Chinese with English abstract).

Liu J, Zhang J, Liu ZH, Yin C, Zhao C, Yu X, Chen Y, Tian Y and Dong Y (2020) Petrogenesis of Permo-Triassic intrusive rocks in Northern Liaoning Province, NE China: implications for the closure of the eastern Paleo-Asian Ocean. *International Geology Review* **62**, 754–80. doi: 10.1080/00206814.2019.1633693.

Liu YJ, Li WM, Ma YF, Feng ZQ, Guan QB, Li SZ, Chen ZX, Liang CY and Wen QB (2021) An orocline in the eastern Central Asian Orogenic Belt. *Earth-Science Reviews* **221**, 103808. doi: 10.1016/j.earscirev.2021.103808.

Liu YS, Wang XH, Wang DB, He DT, Zong KQ, Gao CG, Hu ZC and Gong HJ (2012) Triassic high-Mg adakitic andesites from Linxi, Inner Mongolia: insights into the fate of the Paleo-Asian ocean crust and fossil slab-derived melt–peridotite interaction. *Chemical Geology* **328**, 89–108.

Liu ZC, Wang JG, Liu XC, Liu Y and Lai QZ (2020) Middle Miocene ultrapotassic magmatism in the Himalaya: a response to mantle unrooting process beneath the orogen. *Terra Nova* **33**, 240–51.

Maniar PD and Piccoli PM (1989) Tectonic discrimination of granitoids. *Geological Society of America Bulletin* **101**, 635–43.

Maury RC, Andriambololona R and Dupuy C (1978) Evolution comparée de deux séries alcalines du Pacifique Central: rôle de la fugacité d'oxygène et de la pression d'eau. *Bulletin of Volcanology* **41**, 97–118.

McLennan SM (1993) Weathering and global denudation. *The Journal of Geology* **101**, 295–303.

Miao LC, Fan WM, Liu DY, Zhang FQ, Shi Y and Guo F (2008) Geochronology and geochemistry of the Hegenshan ophiolitic complex: implications for late-stage tectonic evolution of the Inner Mongolia-Daxinganling Orogenic Belt, China. *Journal of Asian Earth Sciences* **32**, 348–70.

Miller C, Schuster R, Kltzli U, Frank W and Purtscheller F (1999) Post-collisional potassic and ultrapotassic magmatism in SW Tibet: geochemical and

Sr–Nd–Pb–O isotopic constraints for mantle source characteristics and petrogenesis. *Journal of Petrology* **40**, 1399–424.

Müller RD, Zahirovic S, Williams SE, Cannon J, Seton M, Bower DJ, Tetley MG, Heine C, Le Breton E, Liu S, Russell SHJ, Yang T, Leonard J and Gurnis M (2019) A global plate model including lithospheric deformation along major rifts and orogens since the Triassic. *Tectonics* **38**, 1884–907.

Nozaka T and Liu Y (2002) Petrology of the Hegenshan ophiolite and its implication for the tectonic evolution of northern China. *Earth and Planetary Science Letters* **202**, 89–104.

Pearce JA (1982) Trace element characteristics of lavas from destructive plate boundaries. In Orogenic Andesites and Related Rocks (ed. RS Thorpe), pp. 528–48. Chichester: John Wiley and Sons.

Peccerillo A and Taylor AR (1976) Geochemistry of Eocene calc-alkaline volcanic rocks from the Kastamonu area, Northern Turkey. *Contributions to Mineralogy and Petrology* **58**, 63–81.

Pitcher WS (1983) Granite type and tectonic environment. In Mountain Building Processes (ed. K Hsu), pp. 19–40. London: Academic Press.

Qian Q and Hermann J (2013) Partial melting of lower crust at 10–15 kbar: constraints on adakite and TTG formation. *Contributions to Mineralogy and Petrology* **165**, 1195–224.

Rapp RP, Shimizu N and Norman MD (2003) Growth of early continental crust by partial melting of eclogite. *Nature* **425**, 605–9.

Ren Q, Zhang S, Gao Y, Zhao H, Wu H, Yang T and Li H (2020) New Middle–Late Permian paleomagnetic and geochronological results from Inner Mongolia and their paleogeographic implications. *Journal of Geophysical Research: Solid Earth* **125**, e2019JB019114. doi: 10.1029/2019JB019114.

Robinson PT, Zhou MF, Hu XF, Reynolds P, Wenji B and Yang JS (1999) Geochemical constraints on the origin of the Hegenshan Ophiolite, Inner Mongolia, China. *Journal of Asian Earth Sciences* **17**, 423–42.

Rudnick R and Gao S (2003) Composition of the continental crust. In *Treatise on Geochemistry Vol. 3* (ed. RL Rudnick), pp. 1–64. Amsterdam: Elsevier.

Rudnick RL (1995) Making continental crust. *Nature* **378**, 571–8.

Rudnick RL and Fountain DM (1995) Nature and composition of the continental crust: a lower crustal perspective. *Reviews of Geophysics* **33**, 267–309.

Samuel MD, Moussa HE and Azer MK (2007) A-type volcanics in Central Eastern Sinai, Egypt. *Journal of African Earth Sciences* **47**, 203–26.

Sengör AMC, Natal'in BA and Burtman VS (1993) Evolution of the Altaid tectonic collage and Paleozoic crustal growth in Eurasia. *Nature* **364**, 299–307.

Shan Q, Niu HC, Yu XY and Zeng Q (2007) Geochemical characteristics, magmatic genesis and tectonic background of the late Paleozoic high potassium and high silicon ignimbrite on the southern margin of Altaid, north Xinjiang. *Acta Petrologica Sinica* **23**, 1721–9 (in Chinese with English abstract).

Shang QH (2004) Occurrences of Permian radiolarians in central and eastern Nei Mongol (Inner Mongolia) and their geological significance to the Northern China Orogen. *Chinese Science Bulletin* **49**, 2613–19.

Song ZG, Han ZZ, Gao LH, Geng HY, Li XP, Meng FX, Han M, Zhong WJ, Li JJ, Du QX, Yan JL and Liu H (2018) Permo-Triassic evolution of the southern margin of the Central Asian Orogenic Belt revisited: insights from Late Permian igneous suite in the Daheishan Horst, NE China. *Gondwana Research* **56**, 23–50.

Sun DY, Wu FY, Zhang YB and Gao S (2004) The final closing time of Xiramuron-Changchun-Yanji plate suture zone: evidence from the Dayushan granitic pluton of Jilin. *Journal of Jilin University (Earth Science Edition)* **34**, 174–81 (in Chinese with English abstract).

Sun SS and McDonough WF (1989) Chemical and isotopic systematics of oceanic basalts: implications for mantle composition and processes. In *Magmatism in Ocean Basins* (eds AD Saunders and MJ Norry), pp. 313–45. Geological Society of London, Special Publication no. 42.

Tang K (1990) Tectonic development of Paleozoic fold belts at the north margin of the Sino-Korean Craton. *Tectonics* **9**, 249–60.

Veksler IV (2004) Liquid immiscibility and its role at the magmatic-hydrothermal transition: a summary of experimental studies. *Chemical Geology* **210**, 7–31.

Veksler IV and Thomas R (2002) An experimental study of B-, P- and F-rich synthetic granite pegmatite at 0.1 and 0.2 GPa. *Contributions to Mineralogy and Petrology* **143**, 673–83.

Wang F, Xing KC, Xu WL, Teng FZ, Xu YG and Yang DB (2021) Permian ridge subduction in the easternmost Central Asian Orogenic Belt: magmatic record using Sr–Nd–Pb–Hf–Mg isotopes. *Lithos* **384–385**, 105966. doi: 10.1016/j.lithos.2021.105966.

Wang YJ (1997) Discovery of Permian radiolarians in ophiolite belt on northern side of Xar Moron River, Nei Monggol and its geological significance. *Acta Palaeontologica Sinica* **36**, 58–70 (in Chinese with English abstract).

Wilde SA (2015) Final amalgamation of the Central Asian Orogenic Belt in NE China: Paleo-Asian Ocean closure versus Paleo-Pacific plate subduction-a review of the evidence. *Tectonophysics* **662**, 345–62.

Williams HM, Turner SP, Pearce JA, Kelley SP and Harris NBW (2004) Nature of the source regions for postcollisional, potassic magmatism in southern and northern Tibet from geochemical variations and inverse trace element modelling. *Journal of Petrology* **45**, 555–607.

Winchester JA and Floyd PA (1977) Geochemical discrimination of different magma series and their differentiation products using immobile elements. *Chemical Geology* **20**, 325–43.

Windley BF, Alexeiev D, Xiao W, Kröner A and Badarch G (2007) Tectonic models for accretion of the Central Asian Orogenic Belt. *Journal of the Geological Society, London* **164**, 31–47.

Wu DD, Li S, Chew D, Liu TY and Guo DH (2021) Permian–Triassic magmatic evolution of granitoids from the southeastern Central Asian Orogenic Belt: implications for accretion leading to collision. *Science China Earth Sciences* **64**, 788–806.

Wu FY, Sun DY, Ge WC, Zhang YB, Grant ML, Wilde SA and Jahn BM (2011) Geochronology of the Phanerozoic granitoids in northeastern China. *Journal of Asian Earth Sciences* **41**, 1–30.

Wu FY, Zhao GC, Sun DY, Wilde SA and Yang JH (2007) The Hulan Group: its role in the evolution of the Central Asian Orogenic Belt of NE China. *Journal of Asian Earth Sciences* **30**, 542–56.

Xiao WJ, Windley BF, Hao J and Zhai MG (2003) Accretion leading to collision and the Permian Solonker suture, Inner Mongolia, China: termination of the central Asian orogenic belt. *Tectonics* **22**, 1069. doi: 10.1029/2002TC001484.

Xiao WJ, Windley BF, Huang BC, Han CM, Yuan C, Chen HL, Sun M, Sun S and Li JL (2009) End-Permian to mid-Triassic termination of the accretionary processes of the southern Altaids: implications for the geodynamic evolution, Phanerozoic continental growth, and metallogeny of Central Asia. *International Journal of Earth Sciences* **98**, 1189–217.

Xiao WJ, Windley BF, Sun S, Li JL, Huang BC, Han CM, Yuan C, Sun M and Chen HL (2015) A tale of amalgamation of three Permo-Triassic collage systems in Central Asia: oroclines, sutures, and terminal accretion. *Annual Review of Earth and Planetary Sciences* **43**, 477–507.

Xin YL, Ren JL, Peng YJ and Sun XQ (2011) Ending of the mountain-building movement of Xing'an-Mongolian-Ji-Hei Orogenic Belt in Northeast China: evidence from Late Triassic molasses (geotectonic phase). *Geology and Resources* **20**, 413–19 (in Chinese with English abstract).

Xu B, Charvet J, Chen Y, Zhao P and Shi GZ (2013) Middle Paleozoic convergent orogenic belts in western Inner Mongolia (China): framework, kinematics, geochronology and implications for tectonic evolution of the Central Asian Orogenic Belt. *Gondwana Research* **23**, 1342–64.

Xu B, Zhao P, Wang Y, Liao W, Luo Z, Bao Q and Zhou Y (2015) The pre-Devonian tectonic framework of Xing'an-Mongolia orogenic belt (XMOB) in north China. *Journal of Asian Earth Sciences* **97**, 183–96.

Yang GX, Li YJ, Tong LL, Wang ZP, Si GH, Lindagato P and Zeng R (2022) Natural observations of subduction initiation: implications for the geodynamic evolution of the Paleo-Asian Ocean. *Geosystems and Geoenvironment* **1**, 100009. doi: 10.1016/j.geogeo.2021.10.004.

Yang JH, Wu FY, Shao JA, Wilde SA, Xie LW and Liu XM (2006) Constraints on the timing of uplift of the Yanshan Fold and Thrust Belt, North China. *Earth and Planetary Science Letters* **246**, 336–52.

Yu Q, Ge WC, Yang H, Zhao GC, Zhang YL and Su L (2014) Petrogenesis of late Paleozoic volcanic rocks from the Daheshen Formation in central Jilin Province, NE China, and its tectonic implications: constraints from geochronology, geochemistry and Sr–Nd–Hf isotopes. *Lithos* **192–195**, 116–31.

Yu Q, Ge WC, Zhang J, Zhao GC, Zhang YL and Yang H (2017) Geochronology, petrogenesis and tectonic implication of Late Paleozoic

https://doi.org/10.1017/S0016756822000358 Published online by Cambridge University Press

volcanic rocks from the Dashizhai Formation in Inner Mongolia, NE China. *Gondwana Research* **43**, 164–77.

Yuan LL, Zhang XH, Xue FH, Lu YH and Zong KQ (2016) Late Permian high-Mg andesite and basalt association from northern Liaoning, North China: insights into the final closure of the Paleo-Asian ocean and the orogen–craton boundary. *Lithos* **258–259**, 58–76.

Zhang DH, Huang BC, Zhao GC, Meert JG, Williams S, Zhao J and Zhou TH (2021) Quantifying the extent of the Paleo-Asian Ocean during the Late Carboniferous to Early Permian. *Geophysical Research Letters* **48**, e2021GL094498. doi: 10.1029/2021GL094498.

Zhang DH, Huang BC, Zhao J, Meert JG, Zhang Y, Liang YL, Bai QH and Zhou TH (2018) Permian paleogeography of the eastern CAOB: paleomagnetic constraints from volcanic rocks in central eastern Inner Mongolia, NE China. *Journal of Geophysical Research: Solid Earth* **123**, 2559–82.

Zhang JH, Gao S, Ge WC, Wu FY, Yang JH, Wilde SA and Li M (2010) Geochronology of the Mesozoic volcanic rocks in the Great Xing'an Range, northeastern China: implications for subduction-induced delamination. *Chemical Geology* **276**, 144–65.

Zhang Q, Wang Y, Li CD, Wang YL and Jia XQ (2006) Granite classification on the basis of Sr and Yb contents and its implications. *Acta Petrologica Sinica* **22**, 2249–69.

Zhang XH, Xue FH, Yuan LL, Ma YG and Wilde SA (2012) Late Permian appinite–granite complex from northwestern Liaoning, North China Craton: Petrogenesis and tectonic implications. *Lithos* **155**, 201–17.

Zhang XH, Zhang HF, Wilde SA, Yang YH and Chen HH (2010) Late Permian to Early Triassic mafic to felsic intrusive rocks from North Liaoning, North China: petrogenesis and implications for Phanerozoic continental crustal growth. *Lithos* **117**, 283–306.

Zhang YB, Wu FY, Wilde SA, Zhai MG, Lu XP and Sun DY (2004) Zircon U–Pb ages and tectonic implications of 'Early Paleozoic' granitoids at Yanbian, Jilin Province, northeast China. *Island Arc* **13**, 484–505.

Zhao P, Appel E, Xu B and Sukhbaatar T (2020) First paleomagnetic result from the Early Permian volcanic rocks in northeastern Mongolia: evolutional implication for the Paleo-Asian Ocean and the Mongol-Okhotsk Ocean. *Journal of Geophysical Research: Solid Earth* **125**, e2019JB017338. doi: 10.1029/2019JB017338.

Zhao P, Chen Y, Xu B, Faure M, Shi G and Choulet F (2013) Did the Paleo-Asian Ocean between North China Block and Mongolia Block exist during the Late Paleozoic? First paleomagnetic evidence from central-eastern Inner Mongolia, China. *Journal of Geophysical Research: Solid Earth* **118**, 1873–94.

Zhou JB, Wilde SA, Zhao GC and Han J (2018) Nature and assembly of microcontinental blocks within the Paleo-Asian Ocean. *Earth-Science Reviews* **186**, 76–93.

Zhou JB, Wilde SA, Zhao GC, Zhang XZ, Wang H and Zeng WS (2010) Was the easternmost segment of the Central Asian Orogenic Belt derived from Gondwana or Siberia: an intriguing dilemma? *Journal of Geodynamics* **50**, 300–17.

Zhou ZB, Pei FP, Wang ZW, Cao HH, Lu SM, Xu WL and Zhou H (2018) Geochronology and geological implications of Fangniugou volcanic rocks in Yitong area, central Jilin Province. *Global Geology* **37**, 46–55 (in Chinese with English abstract).